The Role of Carbonic Anhydrase in Promoting CO_2 Capture and Operation of Bicarbonate-Fed Electrolyzers

by

Yulia Tobolovskaya

A thesis

presented to the University of Waterloo

in fulfillment of the

thesis requirement for the degree of

Master of Science

in

Chemistry

Waterloo, Ontario, Canada, 2022

Author’s Declaration

I hereby declare that I am the sole author of this thesis. This is a true copy of the thesis, including any required final revisions, as accepted by my examiners.

I understand that my thesis may be made electronically available to the public.

Abstract

Capturing CO_2 through chemical absorption offers a sustainable solution to mitigate rising CO_2 emissions which are widely agreed to be the primary contributor to climate change. Among various capture solutions, bicarbonate solvents are favored because they are environmentally clean, have low costs, and low regeneration energies. The main limitation of using these solvents is their slow reaction kinetics with CO_2 which can be improved by the enzyme, carbonic anhydrase through its reversible CO_2 hydration activity. A current focus of research is on developing an integrated CO_2 capture and utilization strategy that is cost-effective, sustainable as well as eco-friendly. Electrochemical conversion of captured CO_2 into commercial products is a promising CO_2 utilization technology that can be directly powered by sustainable renewable energy resources. Unfortunately, regenerating the CO_2 gas feed from the bicarbonate capture medium is currently an energy-intensive, and expensive process. Facilitating this process requires the integration of a bicarbonate-to-CO_2 promoter to directly release CO_2 to the electrocatalytic surface. To this end, the thesis explores a novel bio-electrocatalytic system that feeds CO_2 released through the bicarbonate dehydration activity of the enzyme, bovine carbonic anhydrase to the electrode surface comprising Au branched nanoparticles for its reduction to CO. Through electrochemical and biochemical techniques, we evaluate the performance of two different system configurations operating with external or local scale CO_2 regeneration at the electrocatalytic surface. We show that isolating bovine carbonic anhydrase from the electrolyzer in a concentrated solution of $KHCO_3$ at pH 9 allows it to function efficiently for a limited time resulting in a significant faradaic efficiency of 27 %

for the CO product to be achieved. We learn however, that integrating this enzyme onto the electrode surface creates unique challenges that result in a low CO product yield. To this end, our work provides novel insights into the chemical parameters dictating the performance of bovine carbonic anhydrase and offers a valuable perspective on future research surrounding enzymatic bicarbonate utilization electrolyzers.

Acknowledgements

I would like to thank my supervisors; Prof. Anna Klinkova and Prof. Subha Kalyaanamoorthy for giving me the opportunity to explore an innovative and challenging project that allowed me to develop a diverse range of skills. Their guidance, encouragement, and support throughout my M.Sc. program enabled me to smoothly progress through this work and build valuable research skills. I would also like to express my thanks to Prof. Anna Klinkova for involving me in additional research projects which furthered my knowledge and interest of the electrochemistry and nanoscience fields.

I would like to thank my committee members; Prof. John Honek and Prof. Juewen Liu for their advice and support during my M.Sc. program. I would also like to thank Prof. John Honek for delivering his engaging lectures on enzymes which expanded my knowledge of the field and further inspired my interest in studying enzymes.

I would like to thank Dr. Jury Medvedev for training me on performing electrochemical experiments, working with various lab equipment, and helping me troubleshoot experimental issues. I would like to express my gratitude further for his counsel on the analysis of new experimental data, data presentation, experimental planning and for his extensive support throughout my time in the program. I would also like to thank Xenia Medvedeva for her friendship and for training me to synthesize different electrocatalytic Ag and Au nanoparticles, sharing her experimental insight with me, and providing advice on effectively presenting data. Next, I would like to thank Dr. Neha Saini and Mirfath Sultana Mesbahuddin for introducing me to different protein assays used to assess the stability and activity of carbonic anhydrase

enzymes. I would also like to thank Dr. Nardo Esmeralda Nava Rodriguez for teaching me to work with SDS-PAGE, Bradford Assay and helping me troubleshoot experiments with enzyme encapsulation.

Lastly, I would like to thank the rest of the members from the Klinkova lab and Kalyaanamoorthy lab that I've had the pleasure of working with for their positive attitude and moral support.

Table of Contents

List of Figures

List of Tables

List of Abbreviations

ppm	Parts per million
MEA	Monoethanolamine
CO_2RR	Carbon dioxide reduction reaction
BPM	Bipolar membrane
HER	Hydrogen evolution reaction
FE	Faradaic efficiency
NHE	Normal hydrogen electrode
RHE	Reversible hydrogen electrode
CEM	Cation exchange membrane
BCA	Bovine carbonic anhydrase
Au BNPs	Gold branched nanoparticles
OER	Oxygen evolution reaction
CTAB	Cetyltrimethylammonium bromide
SDS-PAGE	Sodium dodecyl sulfate-polyacrylamide gel electrophoresis
BSA	Bovine serum albumin
p-NPA	*p*-nitrophenyl acetate
p-NP	*p*-nitrophenol

Pb UPD	Lead underpotential deposition
CV	Cyclic voltammetry
GC	Gas chromatography
WAU	Wilbur–Anderson Units
CA	Chronoamperometry
PTFE	polytetrafluoroethylene
SazCA	Carbonic anhydrase from *S. azorense*

Chapter 1
Background

1.1 Introduction

CO_2 emissions are widely agreed to be the primary contributor to global warming among other related environmental problems including frequent extreme weather events, rising sea levels, and ocean acidification [1, 2]. Atmospheric CO_2 levels have rapidly increased from 280 parts per million (ppm) since before the start of the Industrial Revolution to 412 ppm in 2020 as a result of the growing transport and industrial sectors [3]. Moreover, the overall amount of CO_2 in the atmosphere reached 34.9 billion tonnes in 2021 [4]. As a result, mitigating CO_2 emissions to alleviate the harmful environmental effects requires the development of sustainable, cost-effective, and eco-friendly CO_2 capture and utilization strategies, which consist of the extraction of CO_2 from the atmosphere or flue gases followed by its conversion into value-added products.

Presently, CO_2 emissions are mitigated by capturing the released CO_2 and then permanently storing it in deep geological repositories [5]. In general, CO_2 capture technologies can be classified into four different types being pre-combustion capture, direct air capture, post-combustion capture and oxy-fuel combustion capture [6]. Pre-combustion capture involves converting fuel into a gaseous mixture of H_2 and CO_2 through a water-gas shift reactor and then combusting H_2 to generate energy while CO_2 is compressed for transportation to a storage site [6, 7]. In comparison, post-combustion capture separates CO_2 from emitted flue gas which is most commonly done through chemical absorption while direct air capture isolates CO_2 from air [6]. Lastly, oxy-fuel combustion capture involves combusting fuel with pure O_2

gas instead of air which consumes more energy making it a more expensive process [6, 8]. The chemical absorption of CO_2 into aqueous amine solvents such as monoethanolamine (MEA) is the most advanced capture technology [9]. This strategy, however, has several disadvantages due to the solvent's susceptibility to degradation, high regeneration energy, volatility and toxicity issues [9, 10]. Moreover, the estimated operating cost of capturing CO_2 directly from the air in MEA is $ 659 per ton CO_2 which is significant [10]. Instead, bicarbonate solvents have gained attention as the favored CO_2 capture medium. Combined with a rate promoter to increase the reaction kinetics with CO_2, bicarbonate solvents offer a cheaper, and more stable alternative to amine-based solvents with lower regeneration energies [11].

The synthesis of commercial products from captured CO_2 is now a growing research field. Overall, CO_2 has a large variety of applications ranging from carbonated beverages, dry ice, fire extinguishers, process fluids, welding medium, and refrigerants to being used in enhanced oil and gas recovery operations, as well as a feedstock in the synthesis of chemicals and fuels [12]. For instance, CO_2 can be reacted with hydrocarbons oxidizing them to olefins, carboxylic acid, and aldehyde [12, 13]. It also participates in the dry reforming of methane which produces syngas (CO and H_2) from the reaction between CO_2 and CH_4 at high temperatures [14, 15]. The resulting syngas is then used as a precursor to produce useful hydrocarbons and chemical feedstocks. Furthermore, CO_2 can also be reacted with H_2 to produce olefins, methane, formic acid, methanol, and dimethyl ether [12, 13]. Additionally, it is also used in the commercial synthesis of urea through the Bosch–Meiser process which is a major component of nitrogen-enriched fertilizer used worldwide [12, 16].

Biochemical approaches have also been extensively explored for CO_2 utilization including the use of the enzyme, formate dehydrogenase to produce formate in the presence of the nicotinamide adenine dinucleotide cofactor [17]. Formate is a precursor for the synthesis of formic acid derivatives some of which are active ingredients in agricultural fumigants [18]. Other enzymes that utilize CO_2 include malic enzyme, carbon monoxide dehydrogenase and carbonic anhydrase [19, 20, 21]. Malic enzyme catalyzes the reversible oxidation of malate to pyruvate, and CO_2 in the presence of the nicotinamide adenine dinucleotide phosphate cofactor [19]. Malate generated from the reverse reaction between pyruvate and CO_2 is extensively used in textile, food, polymer, agricultural and pharmaceutical industries [22]. The next enzyme, carbon monoxide dehydrogenase catalyzes the reduction of CO_2 to CO which is a feedstock for the Fischer-Tropsch process that produces various hydrocarbons with extensive applications such as in the production of diesel and kerosene fuels [20, 23]. Another commonly studied enzyme that uses the substrate, CO_2 is carbonic anhydrase. This enzyme catalyzes the reversible hydration of CO_2 to bicarbonate at high turnover rates which can be used in CO_2 capture operations to promote CO_2 absorption in bicarbonate-based solvents [21].

Another prospective CO_2 utilization technology is the electrochemical CO_2 reduction reaction (CO_2RR) which reduces this harmful greenhouse gas into a wide array of value-added products [24, 25]. In an aqueous media, CO_2 can be converted to CO, and to a narrow scope of hydrocarbons as well as alcohols. Alternatively, this reaction can be coupled to different organic compounds to produce a wide range of valuable carboxylic acids and other multicarbon products [26]. Moreover, this reaction can be powered by renewable energy resources, such as

solar and wind energies, which represents an efficient way of renewable energy conversion into chemical energy.

To perform the CO_2RR, CO_2 must be recovered from its captured form, which poses an economic challenge when designing a cost effective, and sustainable CO_2 capture and utilization system. In a conventional CO_2 recovery process illustrated in Figure 1, the CO_2 rich capture solvent is first pre-heated in a heat exchanger to 95 °C, then transported to the stripper which desorbs CO_2 at roughly 120 °C releasing it to the gas stream and hence, regenerating the capture solvent [10, 27, 28, 29]. Afterwards, the gas stream is passed through a condenser where water is condensed back into the liquid phase to isolate the CO_2 gas for its subsequent compression and storage into tanks. Overall, this is an expensive, energy-intensive process that must be simplified to improve the economic feasibility of CO_2 recovery for utilization purposes.

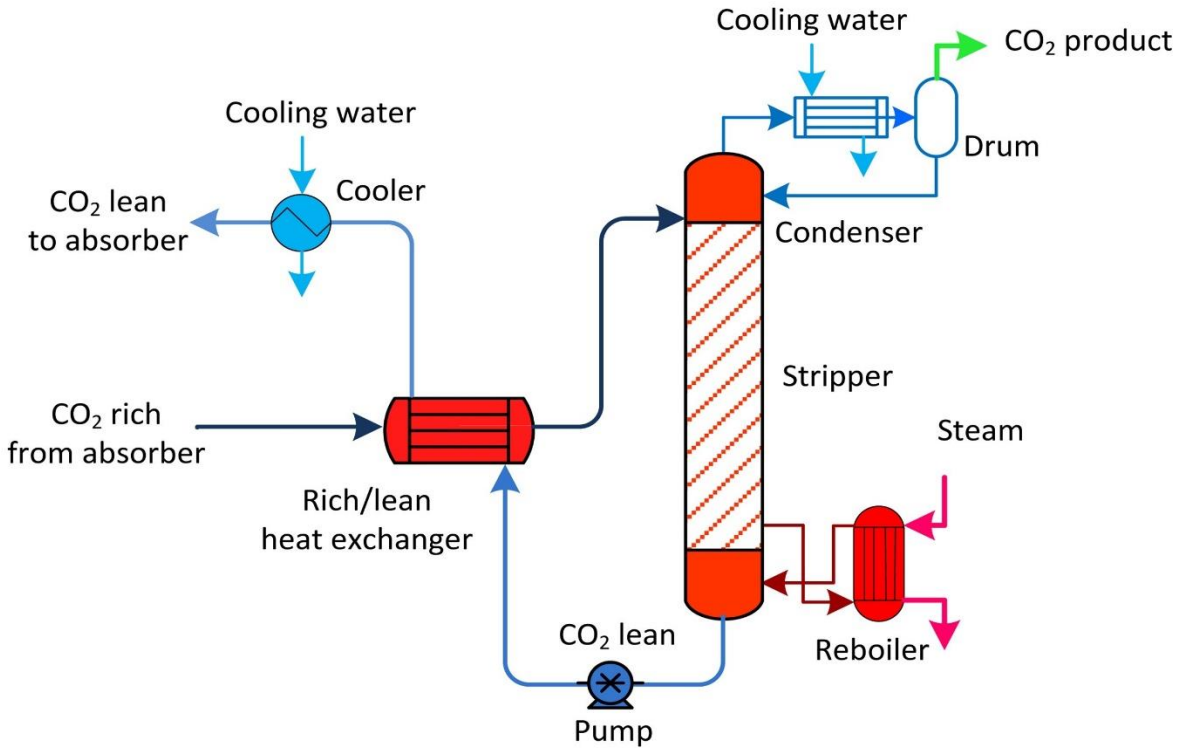

Figure 1. Schematic process flow sheet of the conventional CO_2 stripping system used in capture operations. Reproduced from [27] with permission.

Alternatively, CO_2 can be released from a bicarbonate capture solvent through a chemical reaction occurring between bicarbonate and protons in-situ on a bipolar membrane (BPM) during electrolysis [30]. Unfortunately, there are significant disadvantages of using bipolar membranes which prevent efficient, long-term CO_2 release from being achieved [31]. To elaborate, they exhibit low stability in strong bases, have a short lifetime, are at high risk of delamination, and their manufacturing is an expensive, complex process [31]. Biocatalysts offer another possible route for releasing CO_2 from bicarbonate. In particular, the carbonic anhydrase enzyme is a prime candidate to be used in CO_2RR studies. This zinc containing metalloenzyme catalyzes both the hydration of CO_2 to bicarbonate at high turnover rates relevant in capture operations and the dehydration of bicarbonate back to CO_2 [21]. Exploring

bicarbonate-fed electrolyzers that use carbonic anhydrase to regenerate CO_2 for its electrochemical reduction to value-added products may be key to developing an industrial-scale CO_2 capture and utilization technology.

1.2 The Selective Electrochemical Reduction of CO_2 to CO

Although the electrochemical CO_2RR is a promising CO_2 conversion strategy it is an energy demanding reaction owing to the high stability of the linear CO_2 molecule which comprises a strong C=O bond (750 kJ/mol) [32]. Additionally, it suffers from poor efficiency and selectivity which prevents it from becoming economically feasible at the industrial scale. In general, depending on the number of transferred electrons, CO_2 can be electrochemically converted into various other products, including carbon monoxide, methanol, ethylene, and formic acid. The selectivity of this reaction towards specific products largely depends on the nature of the electrocatalyst employed and the reaction conditions [33, 34, 35]. Among the many different CO_2RR products, CO is especially useful and was assessed to be most economically viable [36, 37]. Specifically, CO is a feedstock for the Fischer-Tropsch process which produces clean liquid hydrocarbons such as diesel and kerosene [23, 25].

The general mechanism of the electrochemical reduction of CO_2 to CO in an aqueous electrolyte can be summarized in four steps [25, 38]. First, CO_2 is adsorbed onto the electrode surface (cathode) and is then reduced to the COOH intermediate through a concerted proton-electron transfer reaction (1.1). COOH is then further reduced by one electron to CO (1.2) which desorbs from the cathode as the final gaseous product. Importantly, instead of desorbing from the electrode surface CO can undergo further C-C coupling or hydrogenation reactions

to form other CO_2RR products. However, to selectively proceed towards the CO product, this reaction requires a suitable electrocatalyst that will strongly bind the key carboxyl intermediate while weakly binding the generated CO to facilitate its release [32]. Additionally, in an aqueous electrolyte, the hydrogen evolution reaction (HER) is a prevalent competing process since it has a similar redox potential to that of the CO_2RR. Briefly, the HER is the formation of H_2 from the electrochemical splitting of water during electrolysis as shown by equation (1.3).

$$CO_2(aq) + H_2O(l) + e^- \rightarrow COOH(aq) + OH^-(aq) \quad (1.1)$$

$$COOH(aq) + e^- \rightarrow CO(aq) + OH^-(aq) \quad (1.2)$$

$$2H_2O(l) + 2e^- \rightarrow H_2 + 2OH^- \quad (1.3)$$

The supporting electrolyte, bicarbonate, also plays a key role in the electrochemical reduction of CO_2 to CO. Dunwell et al. reported that in addition to being the primary carbon source for the CO product, bicarbonate also increases the effective concentration of CO_2 near the electrode surface by facilitating its transportation through a rapid equilibrium exchange mechanism occurring between bicarbonate and CO_2 in solution [38]. Through this process, bicarbonate increases the rate of CO production during electrolysis and improves the efficiency of this electrochemical CO_2RR.

To further increase the efficiency of the electrochemical reduction of CO_2 to CO, the development of stable and selective electrocatalysts is required. To date, Ag and Au nanomaterials are the primary candidates for catalyzing the electrochemical reduction of CO_2 to CO [39, 40, 41]. Many studies confirmed their ability to increase the efficiency of this

reaction by decreasing its large overpotential, increasing its selectivity, and decreasing competition with the HER. In general, the faradaic efficiency (FE) of the CO product reflects the selectivity of these electrocatalysts which refers to the percentage of electrons that participated in the reduction of CO_2 to CO. Although Ag is a cheaper alternative, literature highlights Au to be the preferred choice for CO_2RR studies because it is more stable and more active due to its intrinsically stronger binding of adsorbed C-species [42, 43, 44]. Moreover, it exhibits a higher selectivity towards the CO product, and operates at a lower overpotential [33, 39, 42, 43, 44, 45]. For instance, a bulk Au electrode can achieve a high FE of 91 % for CO at -1.10 V vs the normal hydrogen electrode (NHE) with a partial current density of 3.7 mA cm^{-2} [42]. Moreover, the catalytic properties of Au can be enhanced through the fine tuning of particle size, and surface morphology. Specifically, Zhu et al. looked at the effect of particle size on the resulting surface facets of monodisperse Au nanoparticles [43]. After synthesizing these Au nanoparticles of different sizes, they found that the 8 nm particles exhibited the highest CO FE of 90 % at −0.67 V vs the reversible hydrogen electrode (RHE)) [43]. With evidence from density functional theory calculations, they attributed this high FE of the 8 nm Au nanoparticles to their optimized ratio of edge to corner sites. In general, edge sites favor the formation of CO by stabilizing the carboxyl intermediate while corner sites bind the adsorbed CO strongly preventing its liberation and favor the competing HER [43, 44, 45]. In another study, Zhu et al. synthesized ultrathin Au nanowires comprising a large mass density of the reactive edge sites [45]. As a result, this electrocatalyst reached a FE for CO of 94 % at -0.35 V vs RHE which remained steady for 6 hours thus, demonstrating its durability as well as strong selectivity. Overall these studies highlight the intrinsic properties of Au which make

it a more efficient electrocatalyst than Ag as well as possible enhancements to its activity that can be made through the fine tuning of particle size and surface morphology.

1.3 Liquid Bicarbonate-Fed Electrolyzers

As mentioned previously, the electrochemical reduction of CO_2 to CO is an energy-demanding reaction that primarily operates with a CO_2 gas feed. Integrating this electrochemical utilization technology with CO_2 capture in bicarbonate solvents poses an economic challenge owing to the high-energy CO_2 regeneration steps. To facilitate this process, research efforts are focused on constructing bicarbonate-fed electrolyzers capable of mediating bicarbonate-to-CO_2 conversion to achieve efficient and cost-effective CO production. Currently studied CO_2 desorption mediums capable of promoting the release of CO_2 from the bicarbonate storage medium during electrolysis include the BPM, cation exchange membrane (CEM), and the enzyme, bovine carbonic anhydrase (BCA).

1.3.1 BPM and CEM Bicarbonate-Fed Electrolyzers

Instead of heat-driven desorption, captured CO_2 can be released from the bicarbonate storage medium on a BPM during electrolysis as demonstrated by the Berlinguette group [30]. Figure 2 shows a schematic representation of their BPM containing two-electrode liquid flow-cell electrochemical reactor [30]. The cathodic and anodic compartments of the flow cell contain flow-field plates which are designed to deliver the N_2 saturated $KHCO_3$ and KOH electrolytes to the cathode and anode, respectively. At the nickel foam anode, OH^- is oxidized to O_2 gas while at the Ag nanoparticle-coated porous carbon cathode, bicarbonate is first dehydrated to CO_2 followed by reduction to CO. The BPM plays a vital role in facilitating this

process by enabling the electrochemical splitting of water to occur (1.4) delivering OH^- to the anode and protons to the cathode. These protons react with bicarbonate during electrolysis to generate a high local concentration of CO_2 near the cathode surface (1.5) which is then reduced to CO (1.6) enabling a high faradaic efficiency of 81 % at 25 mA cm^{-2} to be achieved. Additionally, this system overcomes the challenges associated with CO_2 fed aqueous systems including electrolyte acidification which generates conditions that favor the competing HER and the low CO_2 saturation limit which restricts the maximum current density that can be achieved. Unfortunately, there are significant disadvantages of using bipolar membranes including costly and complex manufacturing, short lifetime, low stability in strong bases, and the risk of delamination [31].

$$H_2O(l) \rightarrow H^+(aq) + OH^-(aq) \quad (1.4)$$

$$H^+(aq) + HCO_3^-(aq) \rightarrow CO_2(aq) + H_2O(l) \quad (1.5)$$

$$CO_2(aq) + H_2O(l) + 2e^- \rightarrow CO(g) + 2OH^-(aq) \quad (1.6)$$

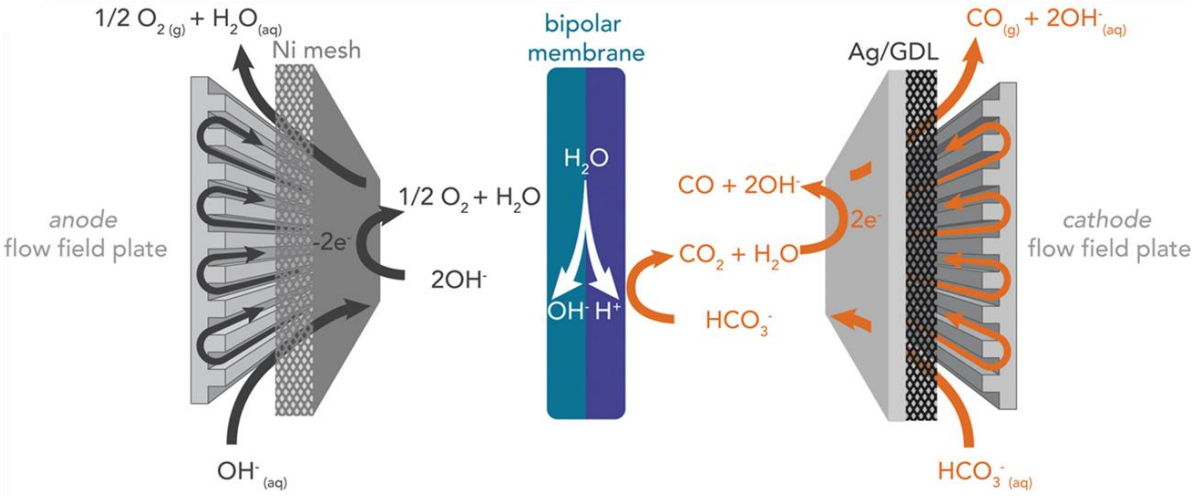

Figure 2. Schematic representation of the flow cell containing a BPM highlighting the relevant chemical and electrochemical reactions occurring at the cathode and anode. Reproduced from [30] with permission.

Alternatively, a CEM may also be used in bicarbonate-fed electrolyzers to achieve the conversion of bicarbonate to CO_2 at the cathode surface. In general, cation exchange membranes are simpler as well as cheaper to manufacture, have a longer lifetime, and higher stability [31]. Similar to the BPM, cation exchange membranes drive the pH-dependent bicarbonate-to-CO_2 equilibrium towards CO_2 formation by transporting H^+ to the cathode to react with bicarbonate. The Berlinguette group reported however, that the CEM containing electrolyzer achieved a lower CO FE of 40 % at 100 mA cm^{-2} than the tested BPM electrolyzer [46]. This lower CO product selectivity can be attributed to the fact that the CEM generates an excess number of protons at the cathode surface which creates acidic conditions that favor the competing HER. Additionally, this electrolyzer relies on a H_2 gas feed being delivered to the anodic compartment to generate the proton flow across the CEM which also prevents this system from becoming economically feasible. Based on these results, other bicarbonate-to-CO_2 conversion mediums will need to be implemented, such as the BCA enzyme, to achieve

efficient CO_2 release and subsequent reduction to the CO product. To specify, BCA can be integrated into an electrolyzer to regenerate CO_2 from the bicarbonate feed through its bicarbonate dehydration activity.

1.3.2 BCA Promoted Bicarbonate-Fed Electrolyzers

BCA is a naturally occurring, single subunit metalloenzyme that promotes CO_2 capture by catalyzing the hydration of CO_2 to bicarbonate and regenerates CO_2 by catalyzing the dehydration of bicarbonate [21]. Overall, this enzyme has a spherical shape with a catalytic active site consisting of a zinc metal ion located near the middle in a cone-shaped cavity as illustrated in Figure 3 [47]. It also has a distinct folding pattern located in the C-terminal region which is referred to as the "knot structure". Molecular dynamics simulation performed by Ohta et al. revealed the formation of this knot structure to be critical to the enzyme's correct folding into the catalytically active structure [47]. Furthermore, they observed that the collection of hydrophobic amino acid residues located on the back of the Zn^{2+} coordination site plays a key role in stabilizing the enzyme's structure and greatly contributes to its mechanical strength. As a result, both the formation of the knot structure and the presence of the hydrophobic cluster are required for the enzyme to enter a catalytically active state.

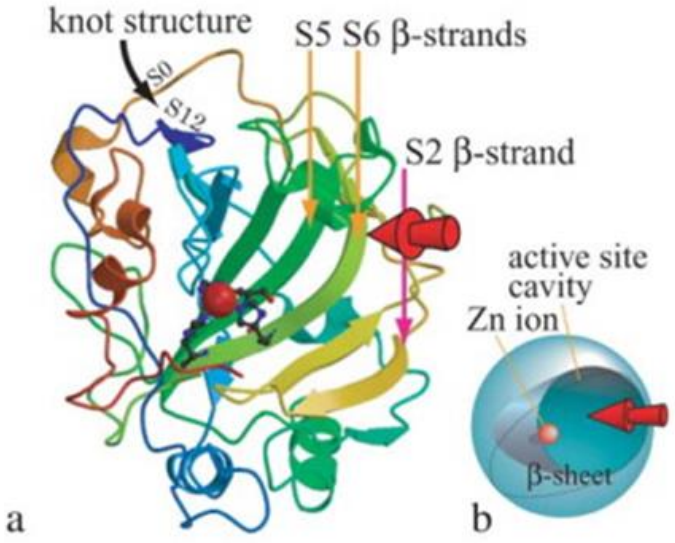

Figure 3. The 3-D structure of BCA obtained from x-ray crystallography (PDB ID: 1V9I). (a) The active site consists of a cone-shaped cavity containing a Zn^{2+} ion as the reaction center which is represented by the red sphere. Stick model shows three histidine residues located in the middle of the β-sheet, and their nitrogen atoms form coordination bonds with the Zn^{2+} ion. The arrow in black shows the ‘‘knot’’ structure in the C-terminal region and the β-strands are represented by the thick multi-colored arrows. (b) A simplified model of the 3-D structure of BCA. Reproduced from [47] with permission.

The ability of BCA to perform its catalytic function originates from Zn^{2+} located at the heart of its reaction center coordinated to three histidine residues. During catalysis, Zn^{2+} coordinates to a water molecule with tetrahedral geometry and facilitates its deprotonation to OH^- by attracting electron density towards itself [21, 48, 49]. As shown in Figure 4, the resulting OH^- then carries out a nucleophilic attack on the CO_2 substrate residing in the hydrophobic pocket of the active site to form the Zn^{2+} -bound bicarbonate ion. This bicarbonate ion then gets displaced by the incoming water molecule whose ionization results in the regeneration of the active site. In this last step of the mechanism, a histidine residue located at the hydrophilic side of the active site acts as a shuttle to remove a proton from the Zn^{2+} -bound water molecule [50]. This histidine residue is part of a network of shuttle residues which are

responsible for facilitating the transfer of a proton from the active site to the surrounding buffer solution which activates BCA for the next cycle of catalysis. Overall, it is agreed that the deprotonation step of the Zn^{2+} -bound water molecule is the rate-determining step [21, 48]. Likewise, this mechanism also proceeds in the reverse direction resulting in the dehydration of bicarbonate to CO_2 gas.

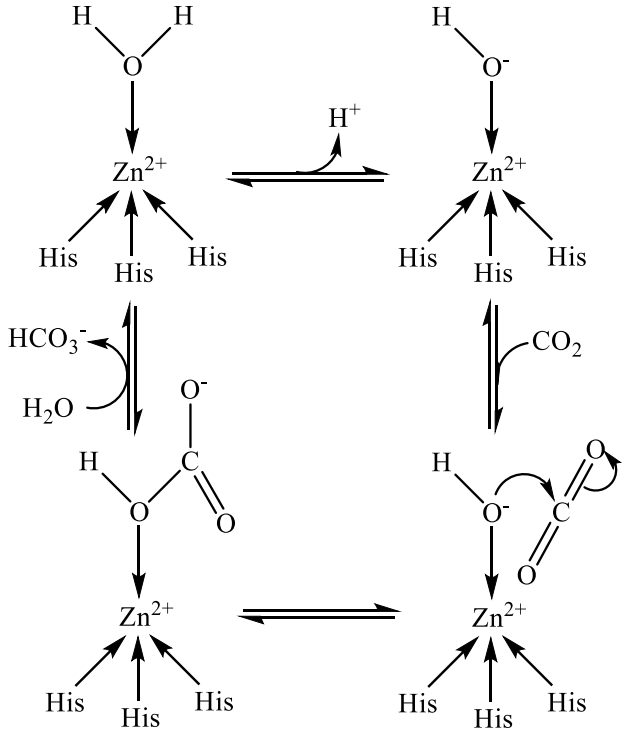

Figure 4. The BCA catalyzed reaction mechanism for the reversible conversion of CO_2 to bicarbonate. Figure was created using ChemDraw.

To date, carbonic anhydrase enzymes have not been used directly in electrochemical CO_2 utilization technologies and the reverse reaction (bicarbonate dehydration to CO_2) is poorly reported on in literature. Earlier studies suggested that the catalytic activity of BCA is dependent upon the ionization state of the Zn^{2+} -bound water molecule in the active site which

in turn, is dependent upon the pH of the surrounding environment [48, 49, 51]. To elaborate, at a higher pH BCA will likely be active towards the hydration of CO_2 because the water molecule will readily ionize to become OH^-. In contrast, at a lower pH this water molecule remains protonated and therefore, BCA will be inactive towards the CO_2 hydration reaction. Instead, the bicarbonate ion will coordinate to the Zn^{2+} replacing the water molecule and the reverse reaction will be catalyzed to generate CO_2. A pH activity curve generated by Donaldson et al. in Figure 5 demonstrates this dependence of the enzyme's catalytic activity on pH by showing that its CO_2 hydration activity decreases with decreasing pH [51]. Furthermore, they established that bicarbonate acts as a noncompetitive inhibitor for binding to the enzyme's active site which suggests that when the concentration of bicarbonate is in excess the enzyme will readily catalyze its conversion to CO_2.

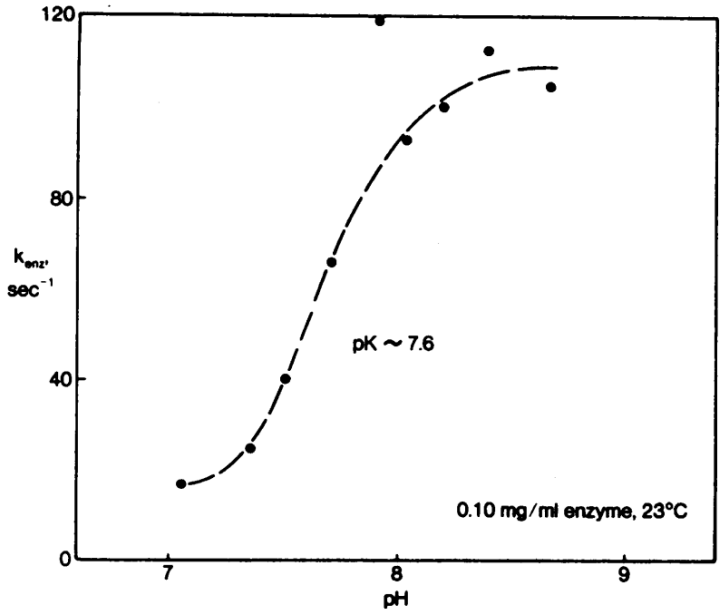

Figure 5. Dependence of the CO_2 hydration activity of BCA on pH in a sodium bicarbonate solvent. Reproduced from [51].

In a recent study, the Berlinguette group attempted to combine CO_2 capture with electrochemical utilization by feeding a capture solution comprising $KHCO_3$, K_2CO_3, and carbonic anhydrase into their BPM electrolyzer [52]. As illustrated in Figure 6, this electrolyzer operates on the same principles as their previously studied BPM electrolyzer (refer to section 1.3.1) to generate CO from a bicarbonate-feed. In contrast to their previous study however, this electrolyzer achieved a low CO FE of 16 % due to the carbonic anhydrase induced deactivation of their Ag electrocatalyst. They unearthed that during electrolysis, carbonic anhydrase chemisorbed onto the electrocatalyst through the thiol groups of its cysteine residues located in its outer shell causing the loss of its electrocatalytic function. As a result, to prevent this enzyme from permeating to the electrocatalytic layer it was recommended to apply a carbon-fiber substrate with a microporous layer over it.

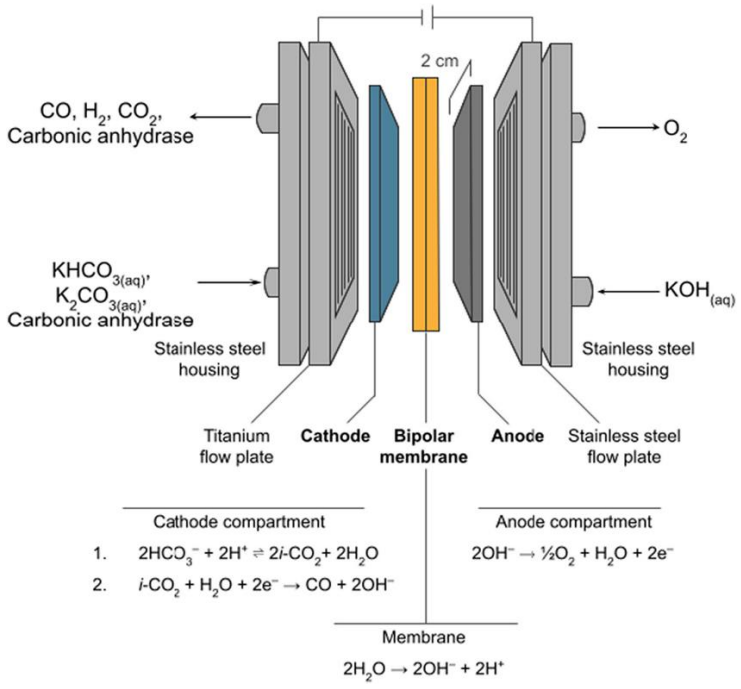

Figure 6. Schematic diagram of the flow cell containing a BPM operating with carbon capture solutions containing carbonic anhydrase. Reproduced from [52] with permission.

In the light of recent findings, combining BCA promoted CO_2 release with electrochemical utilization will require a system configuration that protects BCA from the reaction environment and prevents it from inhibiting the electrocatalyst. Additionally, efforts to directly immobilize BCA on the electrode surface must be taken to improve the economic feasibility of these systems. Immobilization is an innovative approach to recycle enzymes from the reaction environment, reactivate them after partial exhaustion of activity, and stabilize them under high temperature as well as pH conditions [53, 54]. Figure 7 summarizes the five commonly employed enzyme immobilization strategies which include adsorption, covalent bonding, cross-linking, encapsulation, and entrapment [54]. Overall, adsorption is the cheapest and easiest method to use but due to the presence of weak, non-covalent interactions between the enzyme and the support material, it is the least effective strategy. In contrast to adsorption, covalent bonding has been reported to significantly improve the enzyme's stability due to its stronger attachment to the support material through its side chain amino acid and epoxy groups [53]. Furthermore, using cross-linking agents such as glutaraldehyde has been shown to further increase the stability and reusability of enzymes [55]. Encapsulation is another promising immobilization strategy which involves enclosing the enzymes inside a semi-permeable membrane capsule which only allows substrates and products to enter and exit. In general, this strategy has a similar concept to entrapment which involves entrapping enzymes inside the polymeric network of a support material.

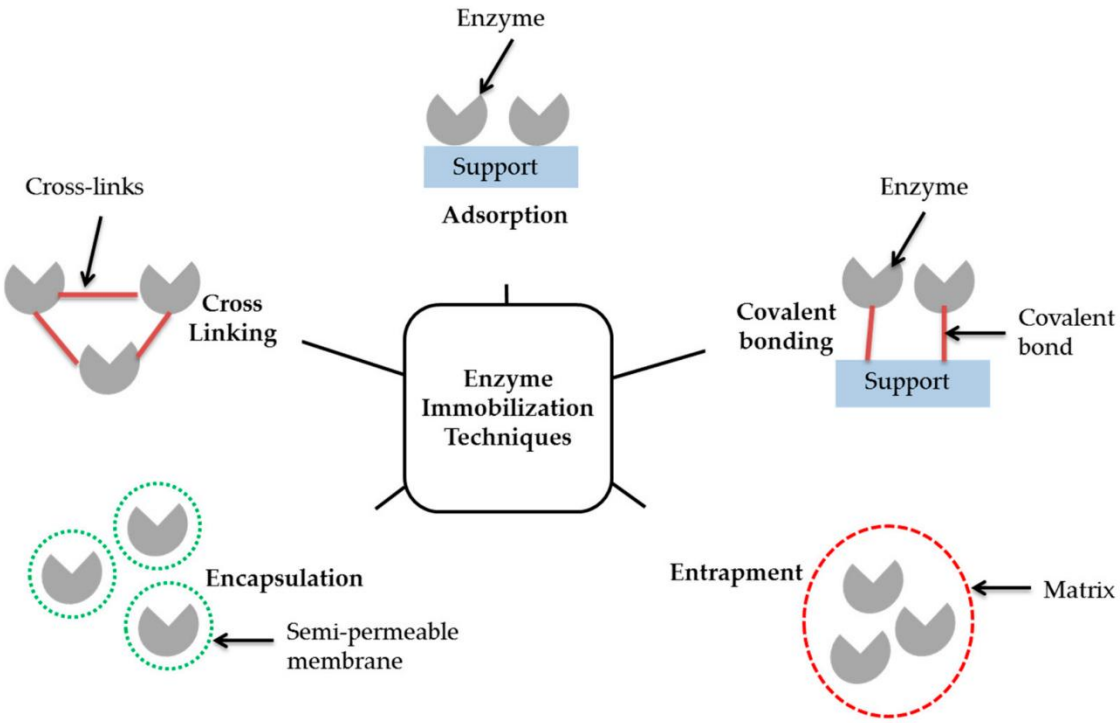

Figure 7. Schematic illustrating the different enzyme immobilization strategies including adsorption, covalent bonding, cross linking, encapsulation and entrapment. Reproduced from [54].

1.4 Scope of Thesis

The thesis explores a novel bio-electrocatalytic system that feeds CO_2 generated from the BCA catalyzed dehydration of bicarbonate to the cathode surface coated with Au branched nanoparticles (Au BNPs) in an H-type electrochemical cell for its efficient reduction to CO. **Chapter 1** delivers the motivation behind this thesis and the relevant background material. **Chapter 2** describes two different BCA promoted electrochemical bicarbonate utilization system configurations along with the experimental methods used to evaluate them. **Chapter 3** focuses on the experimental results pertaining to those electrochemical bicarbonate utilization system configurations. Lastly, **Chapter 4** reveals the conclusions and recommendations for improving the design of this system along with future directions of this work.

Chapter 2

Methods and Materials

2.1 Electrochemical Bicarbonate Utilization System Configurations

The work delivered in this thesis demonstrates a new approach of combining BCA promoted CO_2 release from bicarbonate solvents with electrochemical utilization to improve the economic feasibility of gas-fed electrolyzers. Figure 8 illustrates the schematic process flow of the proposed pathway to bypass the costly, energy-intensive CO_2 regeneration steps present in conventional capture operations to prepare the CO_2 gas feed. To elaborate, first CO_2 from the emitted flue gas is captured through absorption in a bicarbonate solvent but then instead of inducing its desorption through intense heating in a desorber, BCA is used to catalyze the dehydration of bicarbonate back to CO_2. Here, CO_2 gas is released to the cathode coated with Au BNPs that electrocatalyze its reduction to CO.

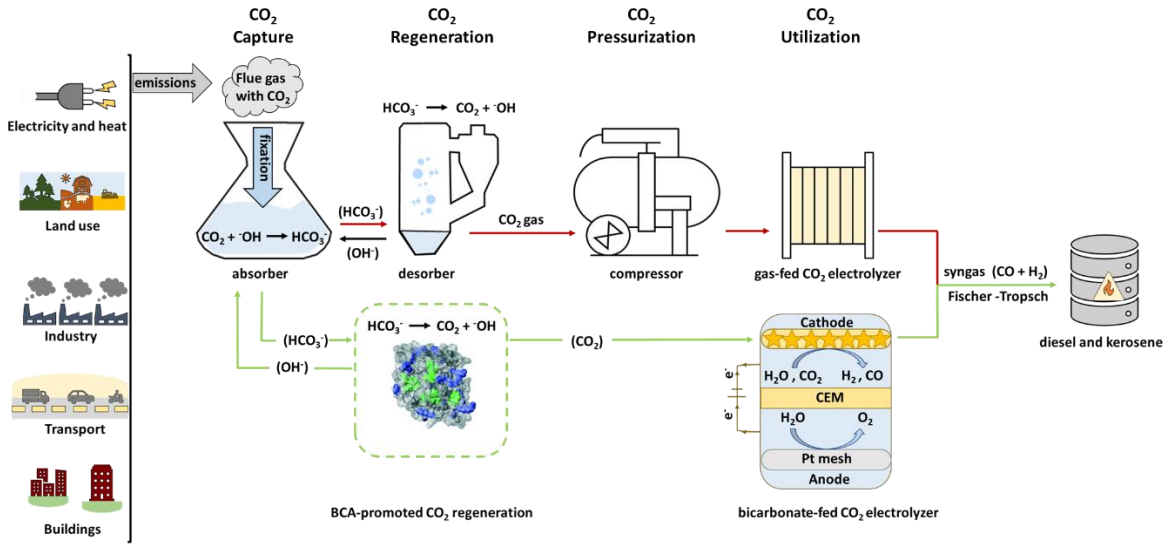

Figure 8. Schematic process flow of proposed pathway (green arrows) from capture to electrochemical utilization using BCA promoted CO_2 regeneration to bypass conventional desorption processes (red arrows). The image of BCA (PDB ID: 1V9E) was reproduced from [56] with permission.

This system was designed in a conventional gas-tight three-electrode H-type electrolytic cell under Ar flow with a 0.5 M potassium bicarbonate electrolyte as illustrated in Figure 9. This electrolytic cell was equipped with a Pt mesh counter electrode (anode) in the anodic compartment, the working electrode (cathode), along with a Ag/AgCl reference electrode in the cathodic compartment and was connected to an electrochemical workstation (Biologic SP-300). The cathode comprising Au BNPs on a carbon support was separated from the anodic compartment by a Nafion CEM which prevents products of the CO_2RR and HER (i.e. CO and H_2) from crossing over to the anodic compartment and getting oxidized at the Pt mesh counter electrode. Likewise, it also prevents O_2 produced at the anode through the oxygen evolution reaction (OER) from crossing-over to the cathode to be reduced which is another undesirable reaction that wastes electrical energy. For this study, Au BNPs were the chosen electrocatalyst due to their high performance and strong selectivity for the desired CO product as a result of their finely tuned nanostructural morphology comprising sharp edges and tips with optimal branch length [57, 58].

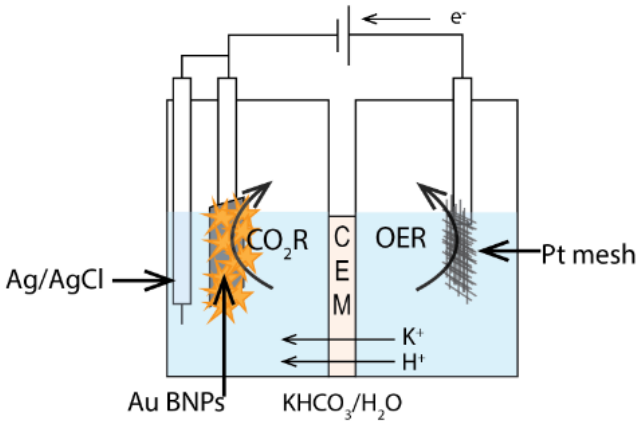

Figure 9. Schematic diagram of an H-type electrolytic cell showing the OER occurring in the anodic compartment and the CO_2RR occurring in the cathodic compartment separated by a CEM.

To integrate BCA into the above electrolyzer to promote CO_2 release, two unique system configurations were explored. Figure 10 (a) illustrates the first configuration where BCA (3.3 mg/mL) in the free form is located in a vial with 2 M $KHCO_3$ outside of the electrolyzer and catalyzes the dehydration of bicarbonate to CO_2 releasing it to the headspace. This regenerated CO_2 is then fed through tubing directly to the Au BNPs cathode surface for its reduction to CO during electrolysis. Figure 10 (b) then shows a local-scale configuration where BCA is directly encapsulated on the cathode surface promoting the release of CO_2 to the Au BNPs. In this configuration, encapsulation was the chosen immobilization strategy because it physically engulfs BCA inside a porous gel material that protects it from the surrounding environment inside the electrolyzer while still enabling substrates and products to freely enter and exit respectively, through the pores, thereby preserving catalytic activity.

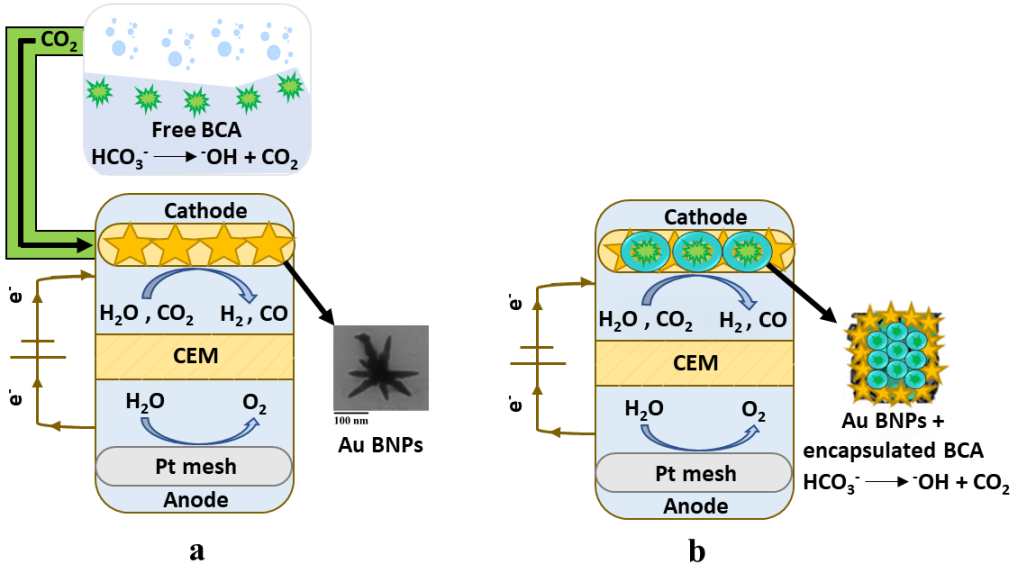

Figure 10. Electrochemical bicarbonate utilization system configurations involving (a) free BCA promoted CO_2 regeneration and (b) local-scale encapsulated BCA promoted CO_2 regeneration. Figure was created using PowerPoint.

2.2 Electrode Fabrication

2.2.1 Synthesis of Au BNPs

Au BNPs were synthesized following a previously established procedure by Choi et al. summarized in Figure 11 [57]. First, Au nanoparticle seeds were prepared by adding 0.5 mL of 10 mM $HAuCl_4$ (Sigma-Aldrich; 99.99 % trace metals basis, 30 wt. % in dilute HCl) to 18 mL of Milli-Q water under intensive stirring followed by 0.5 mL of 10 mM sodium citrate (Sigma-Aldrich; ≥ 99.0 % ACS reagent) and then 0.5 mL of 100 mM $NaBH_4$ (Sigma-Aldrich; powder, ≥ 98.0 %). After 2 more minutes of stirring, the resulting reddish orange solution was left undisturbed for 2-3 hours to age. In the meantime, two growth solutions for the Au BNPs was prepared. The first growth solution was prepared by mixing a solution containing 1 mL of 0.2 M Brij 35 (Thermo Scientific; Waxy solid), and 1 mL of 0.1 M cetyltrimethylammonium bromide (CTAB) with 0.08 mL of 10 mM $HAuCl_4$, 0.01 mL of 5 mM $AgNO_3$ (Sigma-Aldrich; ≥ 99.0 % ACS reagent), 0.2 mL of 50 mM sodium salicylate (Alfa Aesar; 99.0 %), and 0.02 mL of 100 mM ascorbic acid (Sigma-Aldrich; ≥ 99.0 % ACS reagent). Similarly, the second growth solution involved mixing the solution comprising 10 mL of 0.2 M Brij 35, and 10 mL of 0.1 M CTAB (Sigma-Aldrich; ≥ 99.0 %) with 0.8 mL of 10 mM $HAuCl_4$, 0.1 mL of 5 mM $AgNO_3$, 2 mL of 50 mM sodium salicylate, and 0.2 mL of 100 mM ascorbic acid. Lastly, to initiate the development of the Au BNPs, 0.1 mL of the aged Au nanoparticle seeds was added to the first growth solution, briefly shaked, and then 0.1 mL of this resulting reaction mixture was quickly added to the second growth solution and shaken vigorously for 2 min before being left undisturbed overnight. The next day, the supernatant was removed, and the precipitate was

washed twice with centrifugation (3500 g for 10 min). To prepare the catalyst ink, the Nafion-117 solution (Sigma-Aldrich; ~5% in a mixture of water and lower aliphatic alcohols) was added to the washed Au BNPs and sonicated for 30 s. Then this ink was either drop casted onto carbon paper or soaked into the carbon felt support to generate the electrodes for electrolysis. In both cases, once the electrodes were fully dry, they were thoroughly washed with water and methanol to remove any remaining impurities.

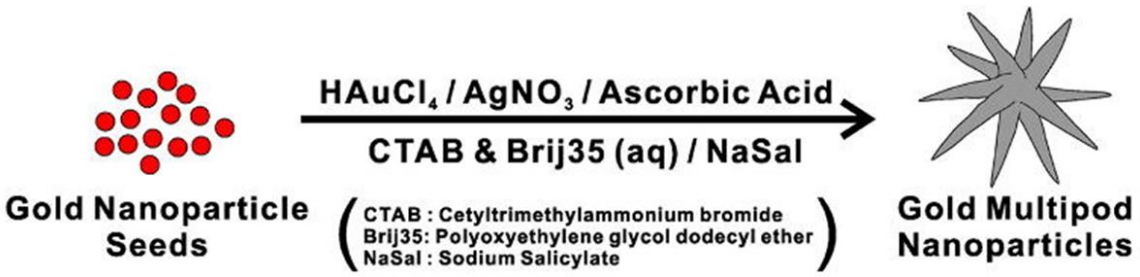

Figure 11. Synthesis of Au BNPs. Reproduced from [57] with permission.

2.2.2 BCA Encapsulation in Silica Gel

Carbonic anhydrase from bovine erythrocytes (≥2,000 W-A units/mg protein) in the lyophilized powder form with a molecular weight of 30 kDA was purchased from Sigma-Aldrich. When not in use, this enzyme in the poly bottle packaging was stored in the fridge at around 4 ^{o}C. To prepare BCA (80 U/mL) for encapsulation in silica gel, 0.4 mg of the lyophilized BCA powder was dissolved in 10 mL of a 16 mM Tris-sulphate buffer solution, pH 7.5 at room temperature. This buffer solution was prepared by dissolving 19.38 mg of the Tris base (EMD Millipore; Molecular biology grade) in 10 mL of Milli-Q water. The desired

pH of this buffer was reached through titration with H_2SO_4 (Sigma-Aldrich; 95-98 % ACS reagent).

The encapsulation of BCA in silica gel was done using a previously established procedure from literature [59]. First, a mixture containing 0.4 mL of 3.37 M tetramethyl orthosilicate (Sigma-Aldrich; ≥99 %) and 0.49 mL of 2.5 mM HCl (Sigma-Aldrich; 37 % ACS reagent) was stirred for 30 min at 40 °C followed by cooling for another 30 min at 4 °C. Next, 0.93 mL of BCA (80 U/mL) was mixed with 0.04 mL of methanol (Sigma-Aldrich; ≥ 99.9 % HPLC grade) and stirred for 5 min before being added to the cooled sol solution made in the previous step. This final solution was then briefly mixed before being sealed with parafilm and left to age at 4 °C for 24 hours. The resulting wet silica gel was then drop casted onto the back side of the carbon paper electrode opposite the Au BNPs which face the CEM during electrolysis and sealed with Nafion.

2.2.3 BCA Encapsulation in Alginate Silica Gel

2.2.3.1 Fabricating the Au BNPs Carbon Felt Electrode with Encapsulated BCA

The encapsulation of BCA in the alginate-silica silica gel can be summarized by the three steps outlined in Figure 12. First the encapsulation mixture was prepared following a previously established procedure from literature [60]. In short, 20 mg of alginic acid sodium salt (Sigma-Aldrich; powder) was dissolved in a mixture containing 0.7 mL of Milli-Q water and 0.2 mL of 0.05 M phosphate buffer pH 7.6. Next, 100 μL of tetraethyl orthosilicate (Sigma-Aldrich; 99.999 % trace metals basis) was added to ensure sufficient cross-linking followed by 3 mg of BCA in the lyophilized powder form. The final concentration of BCA in the resulting

encapsulation mixture was 3 mg/mL. Afterwards, the Au BNPs carbon felt electrode was placed in the glass filter funnel of a suction filtration apparatus and the encapsulation mixture was poured on top. Once this mixture soaked into the pores of the carbon felt material, the suction was terminated, and the resulting electrode was transferred into a 0.2 M $CaCl_2$ (Sigma-Aldrich; ≥ 99.0 % ACS reagent) solution for 20 min to allow precipitation to occur. Afterwards, it was dried and cut along its largest plane into two 1.7 mm thick pieces.

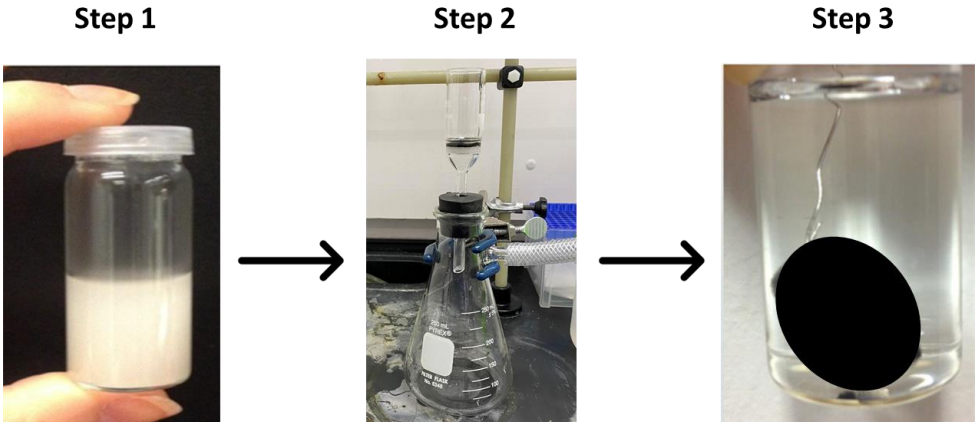

Figure 12. Key steps outlining the encapsulation of BCA on a Au BNPs carbon felt electrode in the alginate-silica gel including the prepared encapsulation mixture with BCA (step 1), suction filtration (step 2), and gel precipitation in $CaCl_2$ (step 3). Step 1 and 3 images were reproduced from [60] with permission.

2.2.3.2 Assessing the Amount of Encapsulated BCA with SDS-PAGE and Bradford Assay

The amount of BCA enzyme encapsulated in the alginate silica gel was assessed qualitatively with sodium dodecyl sulfate-polyacrylamide gel electrophoresis (SDS-PAGE) and quantitatively with the Bradford assay. In SDS-PAGE, sodium dodecyl sulfate will bind to the polypeptide chain of a protein imparting an overall negative charge on it and causing it to denature [61]. This enables protein molecules to be separated based on their molecular weight during electrophoresis where lower molecular weight proteins will migrate further

down the gel towards the positively charged terminal compared to those proteins with a higher molecular weight. For this SDS-PAGE experiment, three samples were prepared including the encapsulated BCA gel, the gel without BCA, and the enzyme in the free form at the expected concentration pertaining to 100 % encapsulation efficiency. Prior to loading the samples in their respective lanes for SDS-PAGE, the gel samples were rehydrated in phosphate buffered saline at 50 ^{o}C and then 20 µL of the rehydrated gel samples along with the free enzyme sample were mixed with 20 µL of BioRad dye. Next, for the Bradford assay 200 µL of the Bradford reagent comprising the Coomassie Brilliant Blue G-250 dye was added to 10 µL of each sample and after a 5 min incubation their absorbance was recorded at 595 nm. In general, this dye disturbs the structure of the protein revealing its hydrophobic pockets to which it will then stably bind to and undergo a color change to blue [62]. Likewise, a series of bovine serum albumin (BSA) standard samples (0-0.5 mg/mL) were also prepared and their absorbance was recorded to generate a standard curve (see Figure A.2 in Appendix). Using the generated equation of the line, the concentration of BCA encapsulated in the gel sample was calculated and compared to the expected concentration at 100 % encapsulation efficiency.

2.2.3.3 Measuring the Esterase Activity of Encapsulated BCA

The esterase activity assay was done to measure and compare the activities of BCA in the encapsulated state and in the free form. In this assay, 100 µL of 30 mM *p*-nitrophenyl acetate (*p*-NPA) (Sigma-Aldrich; esterase substrate) dissolved in acetonitrile (Sigma-Aldrich; ≥ 99.9 % HPLC Plus) was added to the cuvette comprising 900 µL of 22 mM Tris-sulfate buffer pH 7.5 containing the enzyme in the encapsulated or free state at the same concentration

(see Table 1 for full sample composition details) [63]. Following the addition of *p*-NPA, the resulting absorbance change was monitored at 405 nm for 3 min as this substrate was converted into *p*-nitrophenol (*p*-NP). The corresponding control experiments for each trial were also done by adding the *p*-NPA substrate to either the enzyme-free encapsulation gel sample in the buffer solution or to the buffer solution alone. Following equations (2.1-2.4) the amount of the *p*-NP product (mol) produced per min was calculated where A is the absorbance change, E is the extinction coefficient of *p*-NP (16500 M^{-1} cm^{-1}), c is the concentration, l is the pathlength, and V is the volume of the reaction mixture.

$$\Delta A \text{ (absorbance/min)} = (A \text{ of BCA test}) - (A \text{ of control}) \quad 2.1$$

$$\Delta A \text{ (absorbance/min)} = E \text{ (M/cm)} \times \Delta c \text{ (M/min)} \times l \text{ (cm)} \quad 2.2$$

$$[p\text{-NP}] \text{ (M/min)} = \Delta A / 16500 \quad 2.3$$

$$\text{mol of } p\text{-NP produced per min} = [p\text{-NP}] \text{ (M/min)} \times V \quad 2.4$$

Table 1. Compositions of all Prepared Samples in the Esterase Activity Assay

	Trial 1	**Trial 2**	**Trial 3**
Free BCA	100 uL of 30 mM *p*-NPA; 900 uL of 22 mM Tris-sulfate buffer pH 7.5 with free BCA (**0.014 mg/mL** in cuvette)	100 uL of 30 mM *p*-NPA; 900 uL of 22 mM Tris-sulfate buffer pH 7.5 with free BCA (**0.029 mg/mL in cuvette**)	100 uL of 30 mM *p*-NPA; 900 uL of 22 mM Tris-sulfate buffer pH 7.5 with free BCA (**0.011 mg/mL in cuvette**)
Control	100 uL of 30 mM *p*-NPA; 900 uL of 22 mM Tris-sulfate buffer pH 7.5	100 uL of 30 mM *p*-NPA; 900 uL of 22 mM Tris-sulfate buffer pH 7.5	100 uL of 30 mM *p*-NPA; 900 uL of 22 mM Tris-sulfate buffer pH 7.5
Encapsulated BCA	100 uL of 30 mM *p*-NPA; 900 uL of 22 mM Tris-sulfate buffer pH 7.5 comprising the gel sample with BCA (**0.014 mg/mL in cuvette**)	100 uL of 30 mM *p*-NPA; 900 uL of 22 mM Tris-sulfate buffer pH 7.5 comprising the gel sample with BCA (**0.029 mg/mL in cuvette**)	100 uL of 30 mM *p*-NPA; 900 uL of 22 mM Tris-sulfate buffer pH 7.5 comprising the gel sample with BCA (**0.011 mg/mL in cuvette**)
Control	100 uL of 30 mM *p*-NPA; 900 uL of 22 mM Tris-sulfate buffer pH 7.5 comprising the gel sample without BCA	100 uL of 30 mM *p*-NPA; 900 uL of 22 mM Tris-sulfate buffer pH 7.5 comprising the gel sample without BCA	100 uL of 30 mM *p*-NPA; 900 uL of 22 mM Tris-sulfate buffer pH 7.5 comprising the gel sample without BCA

2.2.3.4 Electrochemically Assessing the Impact of the Encapsulated BCA Gel Layer on the Surface Exposure of the Au BNPs Electrocatalyst

To determine if the encapsulated BCA layer was blocking the electrocatalytic surface, lead underpotential deposition (Pb UPD) was done by cyclic voltammetry (CV) in the argon saturated solution of 0.1 M NaOH (Sigma-Aldrich; ≥ 97.0 % pellets ACS reagent) containing 1 mM $Pb(NO_3)_2$ (Sigma-Aldrich; 99.999 % trace metals basis) as described in literature [58]. This experiment was performed with the encapsulated BCA containing Au BNPs electrode, the Au BNPs electrode, and the carbon felt support material (see Figure 20 (b)). Overall, this electrochemical surface characterization technique allows for the crystallographic orientation of the gold surface to be assessed by the electrochemical adsorption of lead. As a result, through visually comparing the three CV curves, the level of exposure of the Au BNPs electrocatalytic surface can be assessed to determine if the encapsulated enzyme gel layer blocked it and thus, disabled its electrocatalytic activity of reducing CO_2 to CO.

2.3 Evaluating the Electrochemical Bicarbonate Utilization System Configurations

2.3.1 BCA Promoted CO_2 Regeneration Configuration

Prior to starting the reaction, the cathodic compartment of the H-type electrolytic cell with the Au BNPs carbon felt electrode was connected through tubing to the headspace of a 20 mL vial containing 50 mg BCA in the lyophilized powder form as demonstrated in Figure 13. Then using a syringe, 15 mL of 2 M $KHCO_3$ (Sigma-Aldrich; 99.5-101.0% acidimetric) was injected into this enzyme-containing vial under stirring and electrolysis began. During electrolysis, gas aliquots from the headspace of the cathodic compartment were extracted under Ar (Praxair; 99.999%) flow (5 scc/min) and analyzed with the Agilent gas chromatography (GC) system every 20 min for 3 hours to calculate the FE of the CO product. Additionally, this experiment was repeated in the absence of BCA to establish the baseline CO FE. Overall, these experiments were performed at -1 V vs Ag/AgCl which is the potential at which the Au BNPs electrocatalyst reduces CO_2 to CO with high selectivity as determined by the control experiments performed under CO_2 saturated conditions (See Figure A.1 (b) in Appendix).

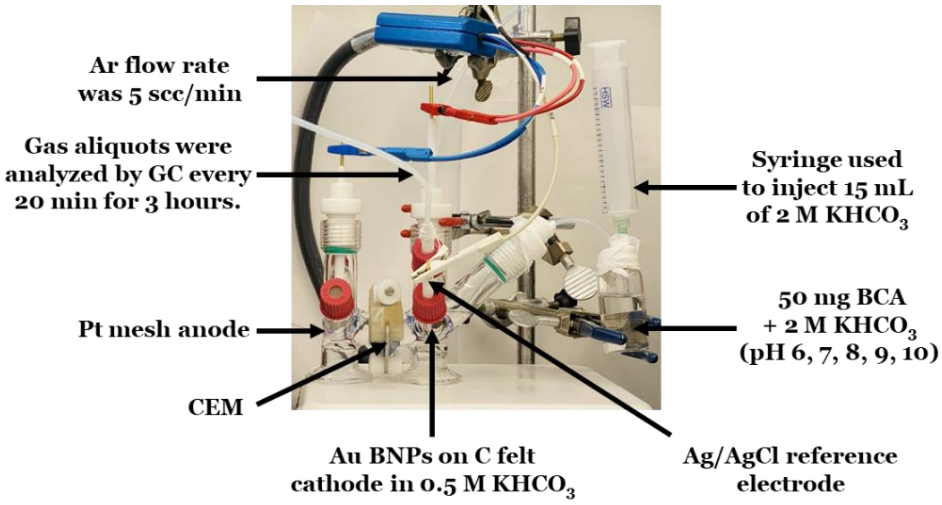

Figure 13. Photo of the experimental set-up for the BCA promoted electrochemical bicarbonate utilization system configuration. The cathodic compartment on the right comprises the Au BNPs working electrode, and the Ag/AgCl reference electrode which are connected to the potentiostat through the red and white alligator clips, respectively. The tubing inserted into the headspace of this compartment enables gas aliquots to be collected for GC analysis under Ar flow (5 scc/min). The cathodic compartment is also connected through tubing to the headspace of the 20 mL vial comprising BCA in 2 M $KHCO_3$ allowing the CO_2 released in this vial to travel directly to the electrocatalytic surface of the cathode. The Nafion CEM separates the cathodic compartment from the anodic compartment on the left which contains the Pt mesh counter electrode that is connected to the potentiostat through the blue alligator clip. In both compartments of this H-cell the electrolyte is 0.5 M $KHCO_3$.

2.3.1.1 Evaluating the Performance of BCA Towards the Bicarbonate Dehydration Reaction at pH 6-10

The activity of BCA was assessed indirectly towards the CO_2 formation reaction at pH 6-10 over 3 hours in the BCA-promoted CO_2 regeneration configuration described above. Here, the pH of the BCA containing 2 M $KHCO_3$ solution was adjusted to 6-8 by the addition of concentrated HCl and to 9-10 by the addition of 5 M KOH (Sigma-Aldrich; ≥ 85 % pellets ACS reagent). Each experiment was also performed in the absence of the BCA enzyme and was done a total of three times to find the deviations of FE of CO and confirm the reproducibility of the data.

2.3.1.2 Assessing the Stability of BCA at pH 6-10

The stability tests were performed by incubating BCA in 20 mM Tris sulfate buffer at pH 6, 7, 8, 9, and 10 prior to testing its activity after the first and third hour using the Wilbur-Anderson CO_2 hydration assay [64]. Briefly, 4 mL of CO_2 saturated water was injected into 6 mL of 20 mM Tris-sulfate buffer pH 8.5. Using a pH meter, the time it takes for the pH of the reaction mixture to change from 8.5 to 6.5 as HCO_3^- forms and H^+ is released was recorded. The activity of BCA (0.0003 mg/mL) was then calculated in Wilbur–Anderson Units (WAU) using equation (2.5) where t_0 is the time for the uncatalyzed reaction to reach pH 6.5 and t_c is the time for the BCA catalyzed reaction to reach pH 6.5.

$$WAU = (t_0 - t_c) / t_c \quad (2.5)$$

2.3.2 Locally Encapsulated BCA Promoted CO_2 Regeneration Configuration

The fabricated Au BNPs carbon paper electrodes comprising encapsulated BCA were all tested in a 0.5 M $KHCO_3$ electrolyte saturated with Ar gas and located in the cathodic compartment of the H-type electrolytic cell shown in Figure 14. To assess the stability and activity of these fabricated electrodes, chronoamperometry (CA) was used together with GC for product analysis. In the CA test, a constant potential of -1.17 V vs Ag/AgCl was applied at the working electrode and the proceeding current response which is dependent on the rate of electrolysis was monitored over time as the reaction progressed. As before, to determine the yield of the CO gas product generated at different times during electrolysis and to calculate its FE, GC analysis of gas aliquots extracted from the headspace of the cathodic compartment was done every 20 min.

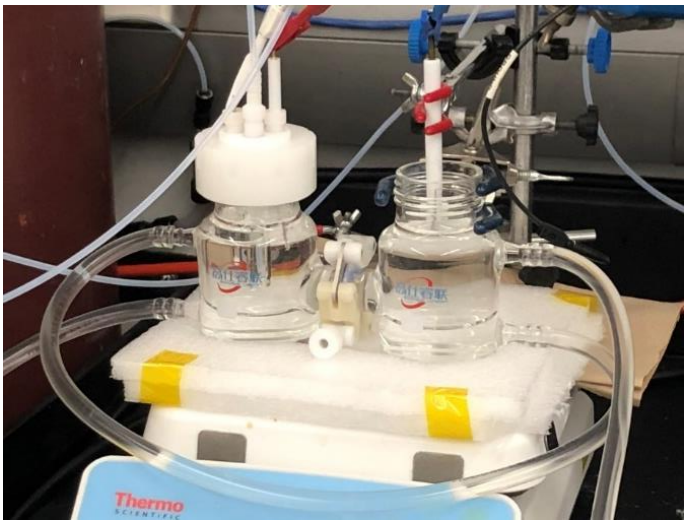

Figure 14. Photo of the experimental set-up for the locally encapsulated BCA promoted electrochemical bicarbonate utilization system configuration. The cathodic compartment on the left comprises the Ar saturated 0.5 M $KHCO_3$ electrolyte along with the encapsulated BCA containing Au BNPs working electrode, and the Ag/AgCl reference electrode which are connected to the potentiostat through the red and white alligator clips, respectively. The Nafion CEM separates the cathodic compartment from the anodic compartment on the right which contains the Pt mesh counter electrode that is connected to the potentiostat through the blue alligator clip. The electrolyte in this compartment is also 0.5 M $KHCO_3$.

Chapter 3
Results

3.1 BCA Promoted Electrochemical Bicarbonate Utilization

The BCA enzyme is a biological catalyst with specific operational conditions meaning that any deviations from optimum temperature or pH within the reaction environment can induce its denaturation and cause activity loss. Keeping this in mind, to develop a successful electrochemical bicarbonate utilization system that relies on BCA promoted CO_2 regeneration, this enzyme must be protected from the reaction environment. One way of preserving BCA is by isolating it from the electrolyzer and another is to encapsulate it on the electrode surface in a gel.

In the first system configuration operating with large-scale CO_2 regeneration, BCA in 2 M $KHCO_3$ (pH 6-10) catalyzed the release of CO_2 to the headspace of a separate compartment from which it traveled through tubing directly to the Au BNPs cathode for its reduction to CO during electrolysis. Figure 15 shows the electrochemical results for this system obtained with and without the BCA enzyme including the CO FE at different times during electrolysis and each experiment's corresponding CA curves. The highest achieved FE for CO was 27 ± 6 % at 20 min during the electrolysis experiment performed with BCA in the pH 9, 2 M $KHCO_3$ solution. This FE represented by the filled blue squares in Figure 15 (a) then decreased to 11 ± 3 % after 3 hours. A similar decay was observed for the experiments done with BCA in the pH 6 and 10 solutions where the CO FE decreased from 9 ± 6 % and 12 ± 4 % to 6 ± 2 % and 7 ± 1 %, respectively over three hours. In contrast, the experiments done with BCA at pH 7

and 8 achieved a more stable but low CO FE in the range of 3-6 % which is not significantly greater than that observed during the control experiments performed without BCA in Figure 15 (b). Overall, these results suggest that BCA was most actively catalyzing the dehydration of bicarbonate to CO_2 in the 2 M $KHCO_3$ solution at pH 9 but was losing its activity as the reaction progressed.

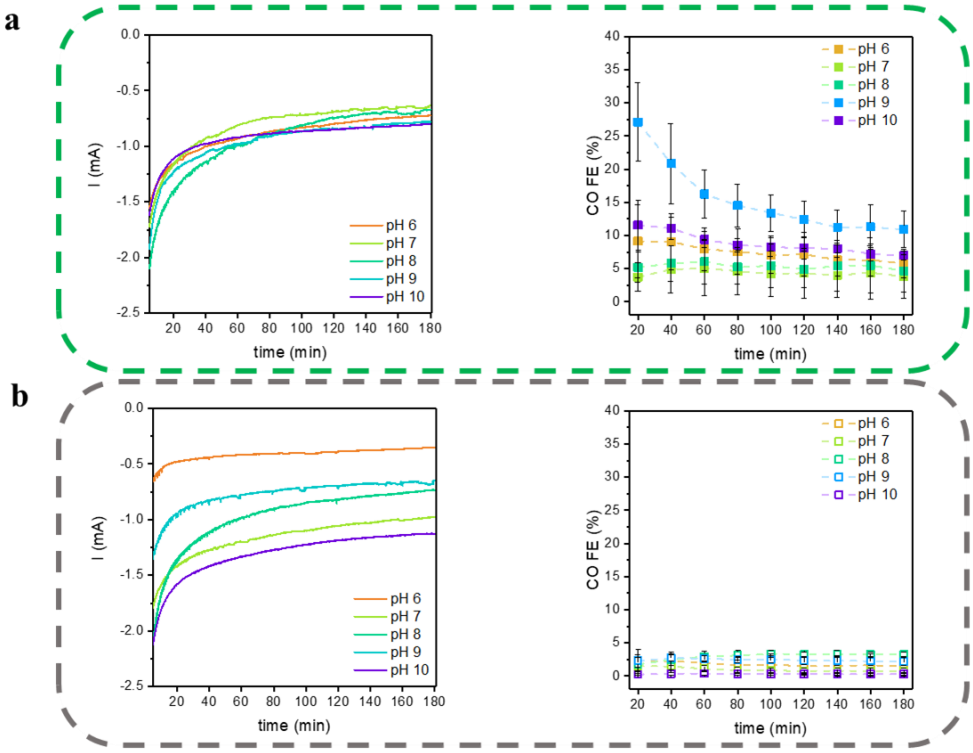

Figure 15. Electrolysis results for the electrochemical bicarbonate utilization system configuration (a) containing BCA and (b) without BCA. The graphs on the left side show the generated CA curves from the electrolysis experiments performed at -1 V vs Ag/AgCl and the graphs on the right side show the corresponding FE for the CO product at different times during each experiment.

The discussed electrochemical bicarbonate utilization system operates on the principles of the pH-dependent CO_2-bicarbonate equilibrium. Depending on the substrate availability and the initial pH, BCA will either drive this equilibrium towards CO_2 or bicarbonate formation [48-51]. As a result, the influence of pH on this enzyme's catalytic CO_2 formation activity was studied. Based on the electrochemical test results obtained at the first hour of electrolysis summarized in Figure 16 (a), BCA was most active towards CO_2 formation at pH 9 but there was no clear linear correlation between the changing pH and the CO FE. Investigations into this enzyme's stability at different pH using the CO_2 hydration assay also demonstrated a decrease in BCA's performance over time after incubation at each pH and revealed it to be most stable in pH 7 as shown in Figure 16 (b). Together these results demonstrate that although the structure of BCA was best preserved under pH 7 conditions, the highest CO product yield during electrolysis was achieved at pH 9. A likely explanation for the increased activity of BCA towards the CO_2 formation reaction at pH 9 is that the low initial CO_2 concentration in solution under these reaction conditions drives BCA to preferably catalyze the dehydration of bicarbonate thus, shifting the equilibrium towards increased CO_2 production [17]. However, since BCA exhibits lower stability at pH 9 it denatures faster and loses its ability to catalyze CO_2 production thus, the CO FE ultimately decreases over time.

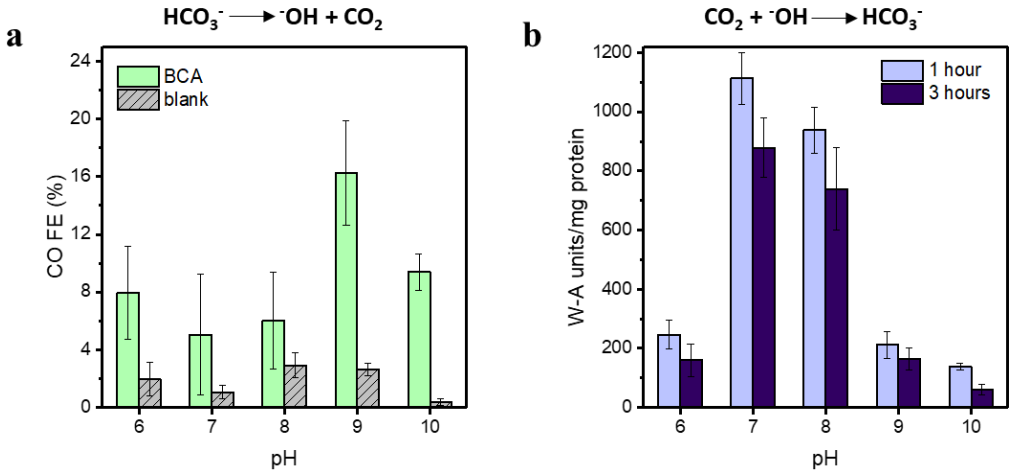

Figure 16. Comparing the performance of BCA at pH 6-10 after (a) 1 hour of electrolysis towards CO_2 formation and (b) incubation in each pH for 1 and 3 hours towards bicarbonate formation.

3.2 Locally Encapsulated BCA Promoted Electrochemical Bicarbonate Utilization

3.2.1 Encapsulated BCA in Silica on a Au BNPs Carbon Paper Electrode

The second studied electrochemical bicarbonate utilization system configuration relies on local-scale BCA promoted CO_2 regeneration at the Au BNPs cathode surface in the Ar saturated 0.5 M $KHCO_3$ electrolyte. The first tested electrode design with BCA encapsulated in silica yielded a CO FE in the range of 19 - 23 % which was higher than that attained by the electrocatalyst electrode without BCA which decreased from 19 to 12 % over 200 min as shown by the filled and empty blue points, respectively in Figure 17. This piece of data demonstrates that BCA was initially stable and actively catalyzing the dehydration of bicarbonate to CO_2 for its reduction to CO during electrolysis in the silica encapsulation material. However, after the peak FE for CO of 23 % was reached with this enzyme electrode at 100 min, it began decreasing along with the magnitude of the current in the corresponding CA curve. This decrease in the CO FE implies that BCA started losing its activity after 100 min because it began denaturing under these reaction conditions or the encapsulated BCA-silica layer was detaching from the electrode surface. Moreover, this achieved CO FE was significantly lower compared to that achieved with the Au BNPs carbon paper electrode under CO_2 saturated conditions in the control experiment (See Figure A.1 (a) in Appendix). As a result, alternative encapsulated-BCA electrode designs need to be explored to improve the efficiency of CO production in this electrochemical bicarbonate utilization system configuration.

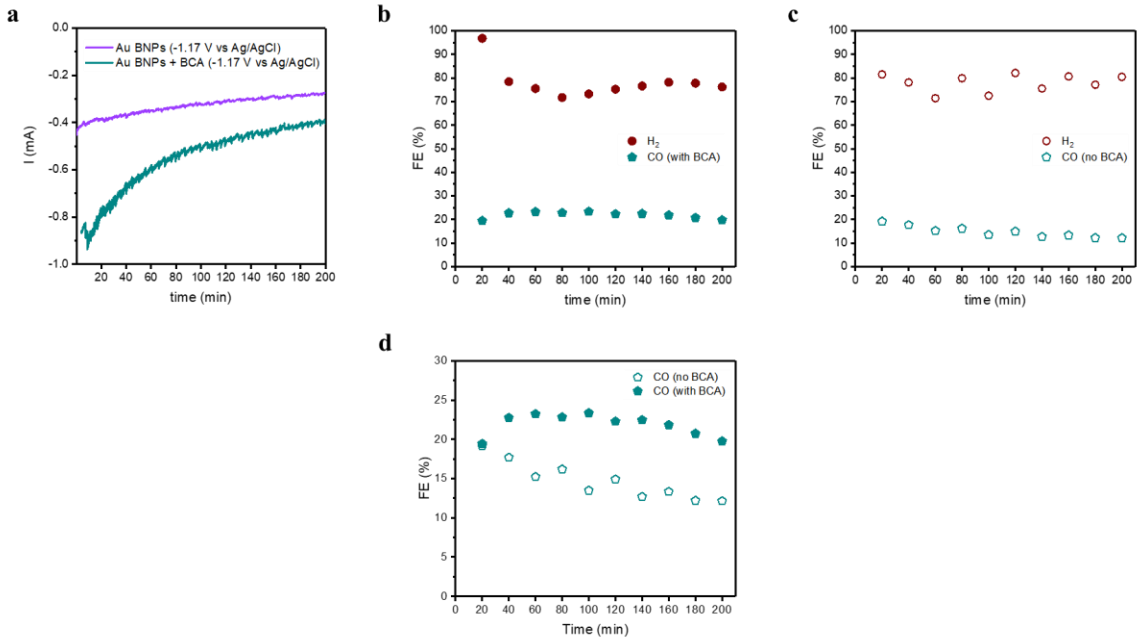

Figure 17. Results for the electrolysis experiments performed in the Ar saturated 0.5 M $KHCO_3$ electrolyte at -1.17 V vs Ag/AgCl with the Au BNPs carbon paper electrode comprising encapsulated BCA and without BCA showing (a) CA curves for the Au BNPs electrode and the encapsulated BCA containing Au BNPs electrode, (b) corresponding FE for CO and H_2 at different times during electrolysis performed with the encapsulated BCA containing Au BNPs electrode and (c) with the Au BNPs electrode without BCA. (d) Comparison of the FE for the CO product achieved with the encapsulated BCA containing Au BNPs electrode and with the Au BNPs electrode in the absence of BCA.

3.2.2 Encapsulated BCA in Alginate Silica on a Au BNPs Carbon Felt Electrode

3.2.2.1 SDS-PAGE and Bradford Assay

Prior to electrochemically testing the second designed electrode, the catalytic performance of BCA encapsulated in the alginate-silica gel was compared to its free form. For a fair comparison, the concentration of BCA encapsulated in the gel was first determined using the Bradford assay. Table 2 reveals the results of this assay which indicate that the concentration of BCA encapsulated in the alginate-silica gel was significantly lower than the expected concentration at 100 % encapsulation efficiency. In general, encapsulation efficiency is defined as the concentration of enzyme detected in the encapsulation gel over the initial enzyme concentration introduced. SDS-PAGE confirmed these results in Figure 18, showing a fainter, smaller band corresponding to the encapsulated enzyme sample in each trial compared to that belonging to the free enzyme sample containing the expected concentration of BCA. Overall, these results show that the encapsulation efficiency was low which can be attributed to the large pore size, and lack of homogeneity of the alginate-silica gel, which causes a significant amount of the enzyme to leach out [60, 65]. In future work, the encapsulation efficiency for this material may be improved by cross-linking BCA with glutaraldehyde [66].

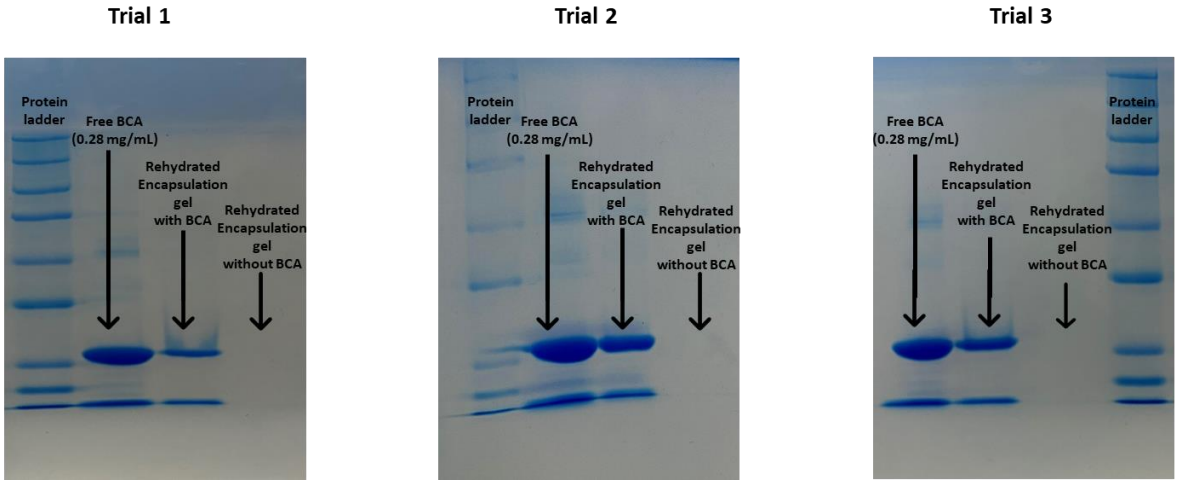

Figure 18. SDS-PAGE results for encapsulated BCA trials 1-3. Each gel shows four columns corresponding to the Protein Ladder with molecular weight markers, the free BCA sample at the expected concentration of BCA pertaining to 100 % encapsulation efficiency, the rehydrated encapsulated BCA sample, and the rehydrated blank sample. Each trial shows a prominent blue band for the free BCA sample, a small band for the rehydrated encapsulated BCA sample, and no band for the rehydrated blank sample.

Table 2. Summary of Bradford Assay Results.

Trial #	Sample	Absorbance at 595 nm	BCA Concentration
1	Gel (no BCA)	0.335	-
1	Free BCA	0.915	0.401
1	Encapsulated BCA	0.412	0.0274
2	Gel (no BCA)	0.327	-
2	Free BCA	0.936	0.444
2	Encapsulated BCA	0.466	0.0579
3	Gel (no BCA)	0.337	-
3	Free BCA	0.863	0.45
3	Encapsulated BCA	0.423	0.0222

3.2.2.2 Esterase Activity Assay

Knowing the concentration of BCA encapsulated in the alginate-silica gel, it was possible to compare its activity to BCA in the free form. Establishing this comparison was important to rule out the possibility of performance issues in the electrochemical bicarbonate utilization system caused by BCA potentially denaturing and losing its ability to catalyze the dehydration of bicarbonate to CO_2 during the procedure that was followed to encapsulate this enzyme in the alginate-silica gel. Figure 19 shows the esterase activity assay results performed with the encapsulated and free BCA samples of equivalent concentration. In both experiments, a similar amount of *p*-NP product was produced over time (μmol of *p*-NP per min) confirming the activity of BCA encapsulated in the alginate-silica gel to be comparable to that of the enzyme in the free state. Based on these results, this encapsulation strategy was established to be compatible with BCA and in turn, to be used in the electrode design for subsequent electrochemical studies.

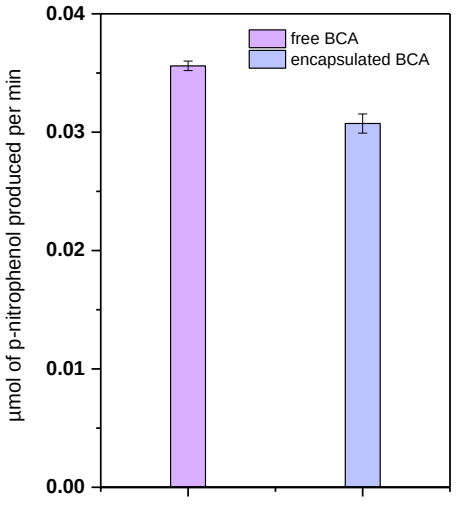

Figure 19. Esterase activity of BCA in the encapsulated and free state.

3.2.2.3 Electrochemical Assessment

As before, the encapsulated BCA containing Au BNPs carbon felt electrode was tested at -1.17 V vs Ag/AgCl in the 0.5 M $KHCO_3$ Ar saturated solution located inside the cathodic compartment of the H-cell. The corresponding electrolysis results in Figure 20 (a) show that a minimal CO FE was attained with this electrode. A likely culprit for this low product yield is the blockage of the electrocatalytic surface by the encapsulated enzyme gel layer which prevents CO_2 reduction from occurring. In other words, even if BCA was successfully catalyzing the formation of CO_2, it was not getting reduced to CO because the activity of the electrocatalyst was disabled. To test this hypothesis, Pb UPD was performed with this electrode and the resulting CV curve was compared to that belonging to the Au BNPs electrode as well as to the carbon felt support material. This electrochemical surface characterization technique assesses the electrode's surface composition which enables the electrocatalyst's level of exposure in the presence of the encapsulated BCA gel layer to be established. Looking at the generated CV curves in Figure 20 (b), the curve for the encapsulated enzyme containing electrode did not have the distinct characteristic peaks related to Au that were observed for the BCA-free Au BNPs electrode. Moreover, it most resembled the curve belonging to the carbon felt support material which ultimately indicates that the encapsulated BCA gel layer is substantially blocking the electrocatalytic layer, hence, preventing it from catalyzing the reduction of CO_2 to CO.

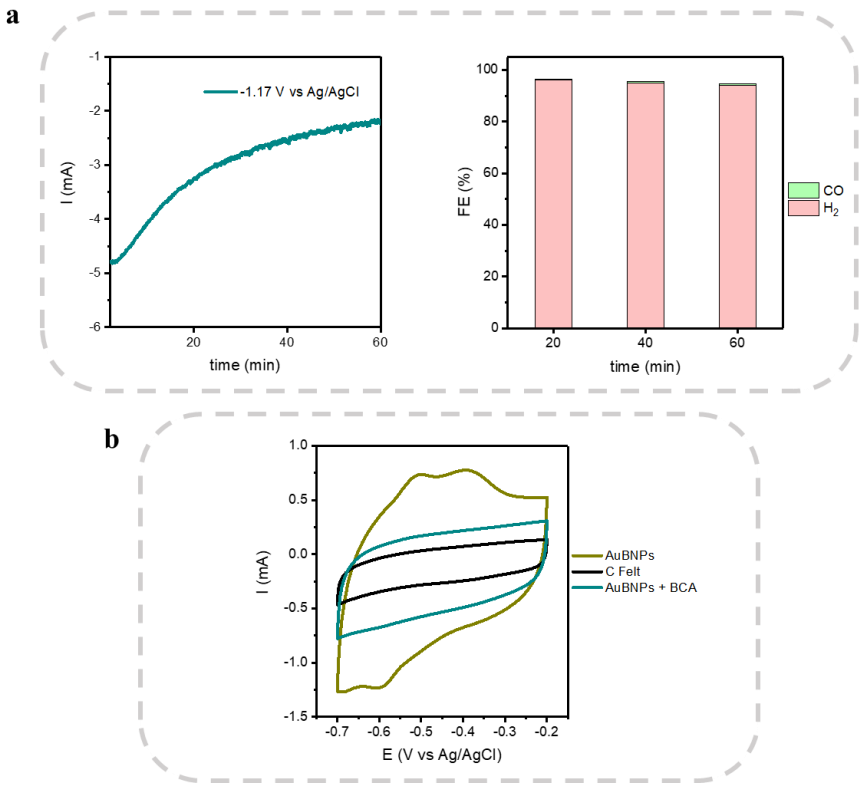

Figure 20. Electrochemical assessment of the encapsulated BCA containing Au BNPs carbon felt electrode including (a) results obtained from the electrolysis experiment performed for 1 hour at -1.17 V vs Ag/AgCl in the Ar saturated 0.5 M $KHCO_3$ electrolyte showing the CA curve in the top left graph and the resulting FE for CO and H_2 in the top right graph, and (b) CV curves generated from the Pb UPD experiment performed with the encapsulated BCA containing Au BNPs electrode, Au BNPs electrode, and carbon felt support material.

3.3 Summary of Chapter 3

In summary, **Chapter 3** presented the experimental work conducted in the assessment of two different system configurations pertaining to the electrochemical bicarbonate utilization electrolyzer. The first examined system configuration relying on the external BCA promoted CO_2 feed achieved a maximum FE for CO of 27 ± 6 % when BCA was kept at pH 9. Unfortunately, the product yield decreased with increasing the time of electrolysis, suggesting that BCA was losing its catalytic activity. Follow-up stability tests conducted by measuring the CO_2 hydration activity of BCA after incubation under different pH conditions confirmed its catalytic activity to be decreasing over time but showed it to be best preserved at pH 7. The second system configuration relying on the local-scale BCA promoted CO_2 feed at the electrode surface achieved a lower FE for CO compared to the previous configuration. Here, performance issues were encountered with both electrode designs. Specifically, in the first design, the silica gel layer comprising BCA likely partially detached from the electrode support during electrolysis. In the second design, the encapsulated BCA layer blocked the electrocatalytic layer which disabled its CO_2 to CO reduction capability. For these reasons, both electrode designs failed to efficiently generate CO by reducing the locally produced CO_2. Outside the scope of this thesis, more intricate enzyme-electrocatalyst designs with an insulated layer for the encapsulated BCA enzyme will need to be explored in the future to generate a higher performance electrochemical bicarbonate utilization system.

Chapter 4
Conclusions and Outlook

4.1 Conclusions and Recommendations

In conclusion, this thesis explored how the BCA enzyme can be integrated into electrochemical bicarbonate utilization electrolyzers to build a sustainable, as well as efficient CO_2 capture and conversion technology. To date, literature did not report on BCA being used directly in electrochemical CO_2RR studies and the chemical parameters surrounding its CO_2 formation activity are poorly understood. In an effort to fill this gap in current scientific research, two different bio-electrocatalytic configurations were studied relying on external and local-scale CO_2 regeneration catalyzed by BCA in the free and encapsulated state, respectively.

From the first system configuration operating with BCA in the free state, we learned that this enzyme actively catalyzes the dehydration of bicarbonate to CO_2 at pH 9 but exhibits short-term stability causing the CO product yield to drop over the course of electrolysis. Next, condensing this system to operate with local CO_2 regeneration at the Au BNPs cathode surface was an important step towards improving its economic feasibility for future applications. In this system, apart from holding BCA at the electrode surface, encapsulation was done to improve this enzyme's reusability, increase its lifespan and stabilize it in harsh environments. Overall, BCA was active in the encapsulation material but did not permit a meaningful CO FE to be achieved compared to the first system configuration. Problems arising from the detachment of the encapsulated enzyme layer from the support and obstruction of the electrocatalytic layer yielded these unfavorable results. As a result, alternative electrode design

options that enable both the enzyme and electrocatalyst to function efficiently over time will need to be explored.

Moving forward based on the results discussed in this thesis, recommendations for improving the enzyme-electrocatalyst electrode design may include the addition of an insulating layer. One example is adding a layer of polytetrafluoroethylene (PTFE) particles onto one side of the Au BNPs electrode support and then anchoring the encapsulated enzyme onto them. This would prevent the applied voltage from damaging BCA while still enabling it to locally catalyze CO_2 formation at the electrode surface without disabling the electrocatalyst. Additionally, this PTFE anchoring agent would further adhere the encapsulated enzyme layer to the electrode support thus, preventing its detachment during electrolysis. Another recommendation is to incorporate the glutaraldehyde cross-linking agent into the selected encapsulation technique to further minimize leaching of the enzyme into the bulk electrolyte during electrolysis and improve reusability. Lastly, a final recommendation is to encapsulate BCA in a polyethyleneimine–polyethylene glycol squalene constitutional framework which in a recent study by Barboiu et al., proved to significantly increase the catalytic proficiency and stability of this enzyme under high temperature conditions [67].

4.2 Outlook

To critically assess the electrochemical bicarbonate utilization system introduced in this thesis for future industrial applications, BCA in its naturally occurring free form is not ideal to operate alongside electrocatalysts to yield profitable CO_2RR products. Apart from easily denaturing under harsh reaction conditions, BCA is expensive, and cannot be recycled from the reaction environment for reuse. Current encapsulation efforts have come a limited way in addressing these challenges. Our electrochemical BCA promoted bicarbonate utilization system, however, paves the way for robust carbonic anhydrase enzymes with enhanced CO_2 formation activity to be used in electrochemical CO_2 utilization technologies. Current research efforts are focused on bioengineering novel carbonic anhydrase enzymes through mutating thermostable variants such as SazCA (carbonic anhydrase from *S. azorense*) to further improve their resilience and catalytic performance [64, 68]. The goal is to build a carbonic anhydrase extremozyme that will efficiently promote CO_2 absorption in bicarbonate capture solvents and actively regenerate CO_2 for conversion. Overall, achieving consistent, long-term CO_2 catalyzed regeneration at the electrode surface of bicarbonate utilization electrolyzers is key to developing a cost-effective integrated system for industrial CO_2 capture and electrochemical utilization that mitigates emissions while also generating value-added commercial products.

Letters of Copyright Permission

ELSEVIER LICENSE
TERMS AND CONDITIONS

Jul 16, 2022

This Agreement between University of Waterloo -- Yulia Tobolovskaya ("You") and Elsevier ("Elsevier") consists of your license details and the terms and conditions provided by Elsevier and Copyright Clearance Center.

License Number	5350901178632
License date	Jul 16, 2022
Licensed Content Publisher	Elsevier
Licensed Content Publication	International Journal of Greenhouse Gas Control
Licensed Content Title	Techno-economic assessment of stripping modifications in an ammonia-based post-combustion capture process
Licensed Content Author	Kangkang Li,Hai Yu,Paul Feron,Leigh Wardhaugh,Moses Tade
Licensed Content Date	Oct 1, 2016
Licensed Content Volume	53
Licensed Content Issue	n/a
Licensed Content Pages	9
Start Page	319
End Page	327

Figure 1. Schematic process flow sheet of the conventional CO_2 stripping system used in capture operations letter of permission.

ELSEVIER LICENSE
TERMS AND CONDITIONS

Jul 16, 2022

This Agreement between University of Waterloo -- Yulia Tobolovskaya ("You") and Elsevier ("Elsevier") consists of your license details and the terms and conditions provided by Elsevier and Copyright Clearance Center.

License Number	5350861298583
License date	Jul 16, 2022
Licensed Content Publisher	Elsevier
Licensed Content Publication	Joule
Licensed Content Title	Electrolytic Conversion of Bicarbonate into CO in a Flow Cell
Licensed Content Author	Tengfei Li,Eric W. Lees,Maxwell Goldman,Danielle A. Salvatore,David M. Weekes,Curtis P. Berlinguette
Licensed Content Date	Jun 19, 2019
Licensed Content Volume	3
Licensed Content Issue	6
Licensed Content Pages	11
Start Page	1487
End Page	1497

Figure 2. Schematic representation of the flow cell containing a BPM highlighting the relevant chemical and electrochemical reactions occurring at the cathode and anode letter of permission.

Figure 3. The 3-D structure of BCA obtained from x-ray crystallography (PDB 1V9I). (a) The active site consists of a cone-shaped cavity containing a Zn^{2+} ion as the reaction center which is represented by the red sphere. Stick model shows three histidine residues located in the middle of the β-sheet, and their nitrogen atoms form coordination bonds with the Zn^{2+} ion. The arrow in black shows the ‘‘knot’’ structure in the C-terminal region and the β-strands are represented by the thick multi-colored arrows. (b) A simplified model of the 3-D structure of BCA. Letter of permission.

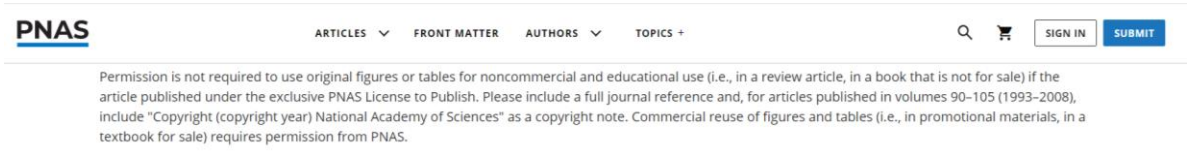

Figure 5. Dependence of the CO_2 hydration activity of BCA on pH in a sodium bicarbonate solvent. Permission is not required.

Jul 16, 2022

This Agreement between University of Waterloo -- Yulia Tobolovskaya ("You") and Elsevier ("Elsevier") consists of your license details and the terms and conditions provided by Elsevier and Copyright Clearance Center.

License Number	5350961389110
License date	Jul 16, 2022
Licensed Content Publisher	Elsevier
Licensed Content Publication	Journal of Inorganic Biochemistry
Licensed Content Title	Electrolytic conversion of carbon capture solutions containing carbonic anhydrase
Licensed Content Author	Arthur G. Fink,Eric W. Lees,Julie Gingras,Eric Madore,Sylvie Fradette,Shaffiq A. Jaffer,Maxwell Goldman,David J. Dvorak,Curtis P. Berlinguette
Licensed Content Date	Jun 1, 2022
Licensed Content Volume	231
Licensed Content Issue	n/a
Licensed Content Pages	1
Start Page	111782

Figure 6. Schematic diagram of the flow cell containing a BPM operating with carbon capture solutions containing carbonic anhydrase letter of permission.

Permissions

Figure 7. Schematic illustrating the different enzyme immobilization strategies including adsorption, covalent bonding, cross linking, encapsulation and entrapment. Permission is not required.

JOHN WILEY AND SONS LICENSE
TERMS AND CONDITIONS

Jul 16, 2022

This Agreement between University of Waterloo -- Yulia Tobolovskaya ("You") and John Wiley and Sons ("John Wiley and Sons") consists of your license details and the terms and conditions provided by John Wiley and Sons and Copyright Clearance Center.

License Number	5351040721577
License date	Jul 16, 2022
Licensed Content Publisher	John Wiley and Sons
Licensed Content Publication	ChemBioChem
Licensed Content Title	Effects of Surface Charge on Denaturation of Bovine Carbonic Anhydrase
Licensed Content Author	George M. Whitesides, Katherine L. Gudiksen, Irina Gitlin
Licensed Content Date	Jul 27, 2006
Licensed Content Volume	7
Licensed Content Issue	8
Licensed Content Pages	10
Type of use	Dissertation/Thesis
Requestor type	University/Academic

Figure 8. The image of BCA (PDB ID: 1V9E) letter of permission.

ELSEVIER LICENSE
TERMS AND CONDITIONS

Jul 16, 2022

This Agreement between University of Waterloo -- Yulia Tobolovskaya ("You") and Elsevier ("Elsevier") consists of your license details and the terms and conditions provided by Elsevier and Copyright Clearance Center.

License Number	5351100810983
License date	Jul 16, 2022
Licensed Content Publisher	Elsevier
Licensed Content Publication	Journal of Colloid and Interface Science
Licensed Content Title	Finely tunable fabrication and catalytic activity of gold multipod nanoparticles
Licensed Content Author	Soon Choi,Youngseo Moon,Hyojong Yoo
Licensed Content Date	1 May 2016
Licensed Content Volume	469
Licensed Content Issue	n/a
Licensed Content Pages	8
Start Page	269
End Page	276
Type of Use	reuse in a thesis/dissertation

Figure 11. Synthesis of Au BNPs letter of permission.

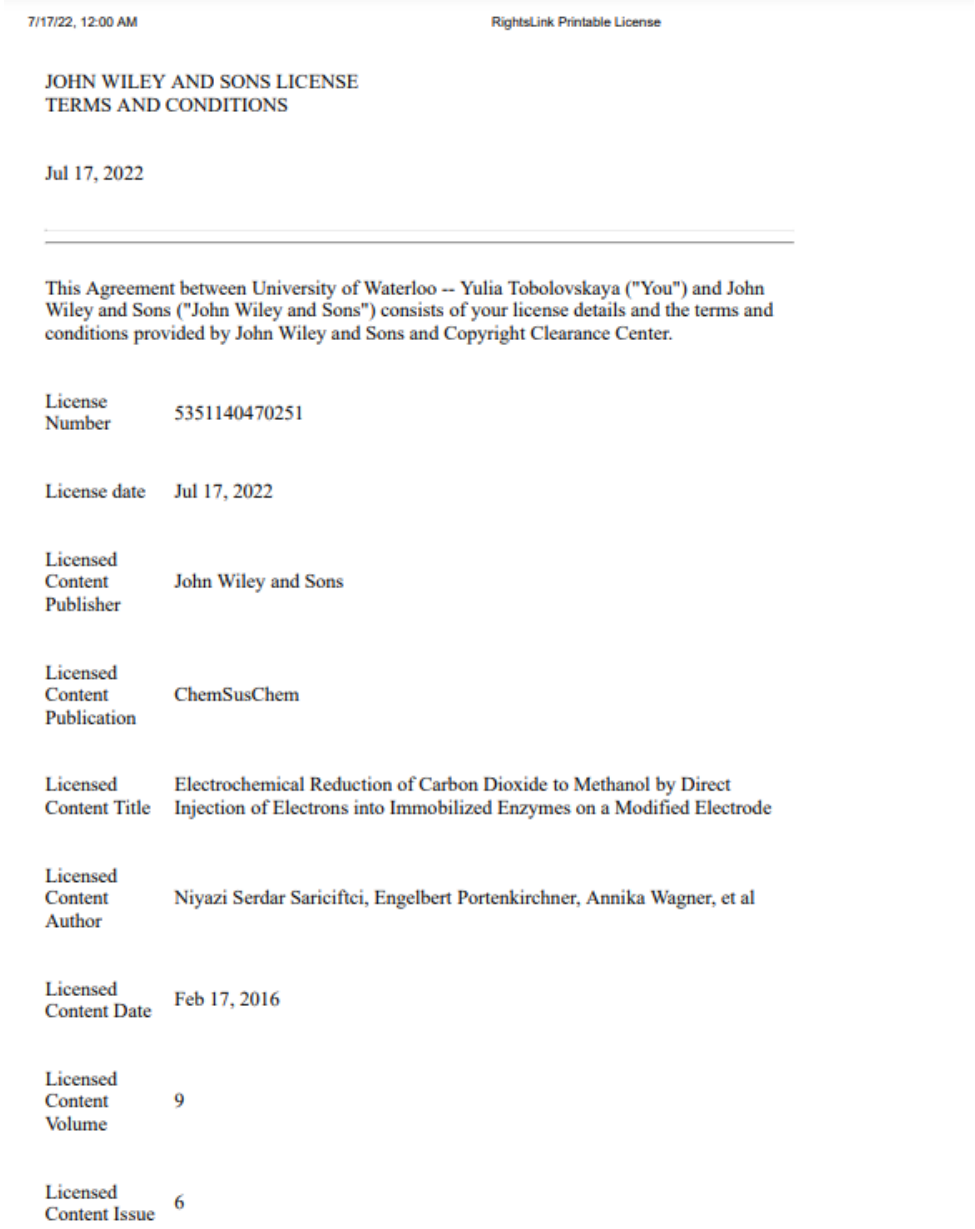

7/17/22, 12:00 AM RightsLink Printable License

JOHN WILEY AND SONS LICENSE
TERMS AND CONDITIONS

Jul 17, 2022

This Agreement between University of Waterloo -- Yulia Tobolovskaya ("You") and John Wiley and Sons ("John Wiley and Sons") consists of your license details and the terms and conditions provided by John Wiley and Sons and Copyright Clearance Center.

License Number	5351140470251
License date	Jul 17, 2022
Licensed Content Publisher	John Wiley and Sons
Licensed Content Publication	ChemSusChem
Licensed Content Title	Electrochemical Reduction of Carbon Dioxide to Methanol by Direct Injection of Electrons into Immobilized Enzymes on a Modified Electrode
Licensed Content Author	Niyazi Serdar Sariciftci, Engelbert Portenkirchner, Annika Wagner, et al
Licensed Content Date	Feb 17, 2016
Licensed Content Volume	9
Licensed Content Issue	6

Figure 12. Key steps outlining the encapsulation of BCA on a Au BNPs carbon felt electrode in the alginate-silica gel including the prepared encapsulation mixture with BCA (step 1), suction filtration (step 2), and gel precipitation in $CaCl_2$ (step 3). Letter of permission for reproducing step 1 and 3 images.

References

1. Kweku DW, Bismark O, Maxwell A, Desmond KA, Danso KB, Oti-Mensah EA, Quachie AT, Adormaa BB: **Greenhouse effect: Greenhouse gases and their impact on global warming.** *JSRR* 2017, **17**:1-9 https://doi.org/10.9734/JSRR/2017/39630.
2. Chiari L, Zecca A: **Constraints of fossil fuels depletion on global warming projections.** *Energy Policy* 2011, **39**:5026-5034 https://doi.org/10.1016/j.enpol.2011.06.011.
3. Erans M, Sanz-Pérez ES, Hanak DP, Clulow Z, Reiner DM, Mutch GA: **Direct air capture: process technology, techno-economic and socio-political challenges.** *Energy Environ. Sci.* 2022, **15**:1360-1405 https://doi.org/10.1039/D1EE03523A.
4. Liu Z, Deng Z, Davis SJ, Giron C, Cias P: **Monitoring global carbon emissions in 2021.** *Nat. Rev. Earth Environ*. 2022, **3**:217-219 https://doi.org/10.1038/s43017-022-00285-w.
5. Zhang S, Liu L, Zhang L, Zhuang Y, Du J: **An optimization model for carbon capture utilization and storage supply chain: A case study in Northeastern China**. *Appl. Energy.* 2018, **231**:194–206 https://doi.org/10.1016/j.apenergy.2018.09.129.
6. Ghiat I, Al-Ansari T: **A review of carbon capture and utilisation as a CO_2 abatement opportunity within the EWF nexus.** *J. CO_2 Util.* 2021, **45**: Article 101432 https://doi.org/10.1016/j.jcou.2020.101432.

7. Raza A, Gholami R, Rezaee R, Rasouli V, Rabiei M: **Significant aspects of carbon capture and storage – a review.** *Petroleum* 2019, **5**:335-340 https://doi.org/10.1016/j.petlm.2018.12.007.
8. Olajire AA: **CO_2 capture and separation technologies for end-of-pipe applications - A review.** *Energy* 2010, **35**:2610-2628 https://doi.org/10.1016/j.energy.2010.02.030.
9. Luis P: **Use of monoethanolamine (MEA) for CO_2 capture in a global scenario: Consequences and alternatives.** *Desalination* 2016, **380**:93–99 https://doi.org/10.1016/j.desal.2015.08.004.
10. Kiani A, Jiang K, Feron P: **Techno-Economic Assessment for CO_2 Capture From Air Using a Conventional Liquid-Based Absorption Process.** *Front. Energy Res.* 2020, **8**: Article 92 https://doi.org/10.3389/fenrg.2020.00092.
11. Ghosh UK, Kentish SE, Stevens GW: **Absorption of carbon dioxide into aqueous potassium carbonate promoted by boric acid**. *Energy Procedia* 2009, **1**:1075–1081 https://doi.org/10.1016/j.egypro.2009.01.142.
12. Rafiee A, Khalilpour KR, Milani D, Panahi M: **Trends in CO_2 conversion and utilization: A review from process systems perspective.** *J. Environ. Chem. Eng.* 2018, **6**:5771-5794 https://doi.org/10.1016/j.jece.2018.08.065.
13. Yang N, Wang R: **Sustainable technologies for the reclamation of greenhouse gas CO2.** *J. Clean. Prod.* 2015, **103**:784-792 https://doi.org/10.1016/j.jclepro.2014.10.025.

14. Abbasi S, Abbasi M, Tabkhi F, Akhlaghi B: **Syngas production plus reducing carbon dioxide emission using dry reforming of methane: utilizing low-cost Ni-based catalysts.** *Oil Gas Sci. Technol*. 2020, **75**: Article 22 https://doi.org/10.2516/ogst/2020016.

15. Saravanan A, Senthil Kumar P, Vo DVN, Jeevanantham S, Bhuvaneswari V, Anantha Narayanan V, Yaashikaa PR, Swetha S, Reshma B: **A comprehensive review on different approaches for CO_2 utilization and conversion pathways.** *Chem. Eng. Sci.* 2021, **236**: Article 116515 https://doi.org/10.1016/j.ces.2021.116515.

16. Glibert PM, Maranger R, Sobota DJ, Bouwman L: **The Haber Bosch–harmful algal bloom (HB–HAB) link.** *Environ. Res. Lett.* 2014, **9**: Article 105001 http://dx.doi.org/10.1088/1748-9326/9/10/105001.

17. Sato R, Amao Y: **Carbonic anhydrase/formate dehydrogenase bienzymatic system for CO_2 capture, utilization and storage.** *React. Chem. Eng*. 2022, **7**:181-191 https://doi.org/10.1039/D1RE00405K.

18. Desmarchelier JM, Johnston FM, Vu LT: **Ethyl formate, formic acid and ethanol in air, wheat, barley and sultanas: analysis of natural levels and fumigant residues.** *Pestic. Sci.* 1999, **55**:815-824 https://doi-org.proxy.lib.uwaterloo.ca/10.1002/(SICI)1096-9063(199908)55:8<815::AID-PS22>3.0.CO;2-4.

19. Häusler RE, Holtum JA, Latzko E: **CO_2 is the inorganic carbon substrate of NADP malic enzymes from Zea mays and from wheat germ.** *Eur. J. Biochem.* 1987, **163**:619-626 https://doi.org/10.1111/j.1432-1033.1987.tb10911.x.

20. Amara P, Mouesca JM, Volbeda A, Fontecilla-Camps JC: **Carbon Monoxide Dehydrogenase Reaction Mechanism: A Likely Case of Abnormal CO_2 Insertion to a Ni−H^- Bond**. *Inorg. Chem.* 2011, **50**:1868–1878 https://doi.org/10.1021/ic102304m.

21. Yong JKJ, Stevens GW, Caruso F, Kentish SE: **The use of carbonic anhydrase to accelerate carbon dioxide capture processes.** *J. Chem. Technol. Biotechnol.* 2015, **90**:3–10 https://doi.org/10.1002/jctb.4502.

22. Jiang Y, Ye X, Zheng T, Dong W, Xin F, Ma J, Jiang M: **Microbial production of L-malate from renewable non-food feedstocks.** *Chin. J. Chem. Eng.* 2021, **30**:105-111 https://doi.org/10.1016/j.cjche.2020.10.017.

23. Gruber H, Groß P, Rauch R, Reichhold A, Zweiler R, Aichernig C, Müller S, Ataimisch N, Hofbauer H: **Fischer-Tropsch products from biomass-derived syngas and renewable hydrogen.** *Biomass Convers. Bioref.* 2021, **11**:2281-2292 https://doi.org/10.1007/s13399-019-00459-5.

24. Zhao X, Du L, You B, Sun Y: **Integrated design for electrocatalytic carbon dioxide reduction**. *Catal. Sci. Technol.* 2020, **10:**2711–2720 https://doi.org/10.1039/D0CY00453G.

25. Medvedev JJ, Tracey C, Engelhardt H, Steksova Y, Krivoshapkin P, Krivoshapkina E, Klinkova A: **Hands-on Electrochemical Reduction of CO_2: Understanding Electrochemical Principles through Active Learning.** *J. Chem. Educ*. 2022, **99:**1036–1043 https://doi.org/10.1021/acs.jchemed.1c01004.

26. Yu J, Wang J, Ma Y, Zhou J, Wang Y, Lu P, Yin J, Ye R, Zhu Z, Fan Z: **Recent Progresses in Electrochemical Carbon Dioxide Reduction on Copper-Based Catalysts toward Multicarbon Products.** *Adv. Funct. Mater.* 2021, **31**: Article 2102151 https://doi.org/10.1002/adfm.202102151.

27. Li K, Yu H, Feron P, Wardhaugh L, Tade M: **Techno-economic assessment of stripping modifications in an ammonia-based post-combustion capture process.** *Int. J. Greenh. Gas Control.* 2016, **53**:319-327. https://doi.org/10.1016/j.ijggc.2016.08.016.

28. Stowe HM, Hwang GS: **Fundamental Understanding of CO_2 Capture and Regeneration in Aqueous Amines from First-Principles Studies: Recent Progress and Remaining Challenges.** *Ind. Eng. Chem. Res.* 2017, **56**:6887−6899 http://dx.doi.org/10.1021/acs.iecr.7b00213.

29. Bos MJ, Kroeze V, Sutanto S, Brilman DWF: **Evaluating Regeneration Options of Solid Amine Sorbent for CO_2 Removal**. *Ind. Eng. Chem. Res.* 2018, **57**:11141−11153 https://doi.org/10.1021/acs.iecr.8b00768.

30. Li T, Lees EW, Goldman M, Salvatore DA, Weekes DM, Berlinguette CP: **Electrolytic conversion of bicarbonate into CO in a flow cell.** *Joule.* 2019, **3**:1487–1497 https://doi.org/10.1016/j.joule.2019.05.021.

31. Ramdin M, Morrison ART, Groen M, Haperen R, Kler R, Broeke LJP, Trusler JPM, Jong W, Vlugt TJH: **High Pressure Electrochemical Reduction of CO_2 to Formic Acid/Formate: A Comparison between Bipolar Membranes and Cation Exchange Membranes.** *Ind. Eng. Chem. Res.* 2019, **58**:1834−1847 https://doi.org/10.1021/acs.iecr.8b04944.

32. Wu J, Huang Y, Ye W, Li Y: **CO_2 Reduction: From the Electrochemical to Photochemical Approach**. *Adv. Sci*. 2017, **4**: Article 1700194 https://doi.org/10.1002/advs.201700194.

33. Nitopi S, Bertheussen E, Scott SB, Liu X, Engstfeld AK, Horch S, Seger B, Stephens IEL, Chan K, Hahn C, Nørskov JK, Jaramillo TF, Chorkendorff I: **Progress and Perspectives of Electrochemical CO_2 Reduction on Copper in Aqueous Electrolyte.** *Chem. Rev.* 2019, **119**:7610–7672 https://doi.org/10.1021/acs.chemrev.8b00705.

34. Pei Y, Zhong H, Jin F: **A brief review of electrocatalytic reduction of CO_2— Materials, reaction conditions, and devices.** *Energy Sci. Eng.* 2021, **9**:1012-1032 https://doi.org/10.1002/ese3.935.

35. Garg S, Li M, Weber AZ, Ge L, Li L, Rudolph V, Wang G, Rufford TE: **Advances and challenges in electrochemical CO_2 reduction processes: an engineering and design perspective looking beyond new catalyst materials.** *J. Mater. Chem. A* 2020, **8**:1511-1544 https://doi.org/10.1039/C9TA13298H.

36. Verma S, Kim B, Jhong HR, Ma S, Kenis PJA: **A Gross-Margin Model for Defining Technoeconomic Benchmarks in the Electroreduction of CO_2.** *ChemSusChem.* 2016, **9**:1972 – 1979 https://doi.org/10.1002/cssc.201600394.

37. Weekes DM, Salvatore DA, Reyes A, Huang A, Berlinguette, CP: **Electrolytic CO_2 reduction in a flow cell.** *Acc. Chem. Res.* 2018, **51**:910–918 https://doi.org/10.1021/acs.accounts.8b00010.

38. Dunwell M, Lu Q, Heyes JM, Rosen J, Chen JG, Yan Y, Jiao F, Xu B: **The central role of bicarbonate in the electrochemical reduction of carbon dioxide on gold.** *J. Am. Chem. Soc.* 2017, **139**:3774–3783 https://doi.org/10.1021/jacs.6b13287.

39. Park JW, Choi W, Noh J, Park W, Gu GH, Park J, Jung Y, Song H: **Bimetallic Gold−Silver Nanostructures Drive Low Overpotentials for Electrochemical Carbon Dioxide Reduction.** *ACS Appl. Mater. Interfaces* 2022, **14**:6604–6614 https://doi.org/10.1021/acsami.1c20852.

40. Kim C, Jeon HS, Eom T, Jee MS, Kim H, Friend CM, Min BK, Hwang YJ: **Achieving Selective and Efficient Electrocatalytic Activity for CO_2 Reduction Using Immobilized Silver Nanoparticles.** *J. Am. Chem. Soc.* 2015, **137**:13844–13850 https://doi.org/10.1021/jacs.5b06568.

41. Ma L, Hu W, Pan Q, Zou L, Zou Z, Wen K, Yang H: **Polyvinyl alcohol-modified gold nanoparticles with record-high activity for electrochemical reduction of CO_2 to CO.** *J. CO_2 Util.* 2019, **34**:108–114 https://doi.org/10.1016/j.jcou.2019.06.002.

42. Hori Y, Murata A, Kikuchi K, Suzuki S: **Electrochemical reduction of carbon dioxides to carbon monoxide at a gold electrode in aqueous potassium hydrogen carbonate.** *J Chem. Soc., Chem. Commun.* 1987, 728-729 https://doi.org/10.1039/C39870000728.

43. Zhu W, Michalsky R, Metin Ö, Lv H, Guo S, Wright CJ, Sun X, Peterson AA, Sun S: **Monodisperse Au Nanoparticles for Selective Electrocatalytic Reduction of CO_2 to CO**. *J. Am. Chem. Soc.* 2013, **135**: 16833−16836 https://doi.org/10.1021/ja409445p.

44. Back S, Yeom MS, Jung Y: **Active Sites of Au and Ag Nanoparticle Catalysts for CO_2 Electroreduction to CO.** *ACS Catal.* 2015, **5**:5089-5096 http://dx.doi.org/10.1021/acscatal.5b00462.

45. Zhu W, Zhang YJ, Zhang H, Lv H, Li Q, Michalsky R, Peterson AA, Sun S: **Active and selective conversion of CO_2 to CO on ultrathin Au nanowires.** *J. Am. Chem. Soc*. 2014, **136**:16132-16135 http://dx.doi.org/10.1021/ja5095099.

46. Zhang Z, Lees EW, Ren S, Mowbray BAW, Huang A, Berlinguette CP: **Conversion of Reactive Carbon Solutions into CO at Low Voltage and High Carbon Efficiency**. *ACS Cent. Sci.* 2022, **8**:749-755 https://doi.org/10.1021/acscentsci.2c00329.

47. Ohta S, Alam MT, Arakawa H, Ikai A: **Origin of mechanical strength of bovine carbonic anhydrase studied by molecular dynamics simulation.** *Biophys. J.* 2004, **87**:4007–4020 https://doi.org/10.1529/biophysj.104.045138.

48. Park D, Lee MS: **Kinetic study of catalytic CO_2 hydration by metal-substituted biomimetic carbonic anhydrase model complexes.** *R. Soc. open Sci.* 2019, **6**: Article 190407 https://doi.org/10.1098/rsos.190407.

49. Zhang YT, Zhang L, Chen HL, Zhang HM: **Selective separation of low concentration CO_2 using hydrogel immobilized CA enzyme based hollow fiber membrane reactors.** *Chem. Eng. Sci.* 2010, **65**:3199–3207 https://doi.org/10.1016/j.ces.2010.02.010.

50. Becker HM, Klier M, Schüler C, Deitmer JW: **Intramolecular proton shuttle supports not only catalytic but also noncatalytic function of carbonic anhydrase II**. *PNAS* 2011, **108**:3071-3076 https://doi.org/10.1073/pnas.1014293108.

51. Donaldson, TL, Quinn, JA: **Kinetic constants determined from membrane transport measurements: carbonic anhydrase activity at high concentrations.** *Proc. Nat. Acad. Sci. USA* 1974, **71**:4995–4999 https://doi.org/10.1073/pnas.71.12.4995.

52. Fink AG, Lees EW, Gingras J, Madore E, Fradette S, Jaffer SA, Goldman M, Dvorak DJ, Berlinguette CP: **Electrolytic conversion of carbon capture solutions containing carbonic anhydrase.** *J. Inorg. Biochem.* 2022, **231**: Article 111782 https://doi.org/10.1016/j.jinorgbio.2022.111782.

53. Effendi SSW, Ng IS: **The prospective and potential of carbonic anhydrase for carbon dioxide sequestration: A critical review.** *Process Biochem.* 2019, **87**:55–65 https://doi.org/10.1016/j.procbio.2019.08.018.

54. Mokhtar NF, Rahman RNZR, Noor NDM, Shariff FM, Ali MSM**: The Immobilization of Lipases on Porous Support by Adsorption and Hydrophobic Interaction** *Catalysts* 2020, **10**: Article 744 https://doi.org/10.3390/catal10070744.

55. Vinoba M, Bhagiyalakshmi M, Jeong SK, Yoon Y, Nam SC: **Immobilization of carbonic anhydrase on spherical SBA-15 for hydration and sequestration of CO_2.** *Colloids Surf. B* 2012, **90**:91–96 https://doi.org/10.1016/j.colsurfb.2011.10.001.

56. Gitlin I, Gudiksen KL, Whitesides GM: **Effects of Surface Charge on Denaturation of Bovine Carbonic Anhydrase.** *ChemBioChem* 2006, **7**:1241-1250 https://doi-org.proxy.lib.uwaterloo.ca/10.1002/cbic.200600191.

57. Choi S, Moon Y, Yoo H: **Finely tunable fabrication and catalytic activity of gold multipod nanoparticles.** *J. Colloid Interface Sci.* 2016, **469**:269–276 https://doi.org/10.1016/j.jcis.2016.02.019.

58. Li F, Medvedeva XV, Medvedev JJ, Khairullina E, Engelhardt H, Chandrasekar S, Guo Y, Jin J, Lee A, Thérien-Aubin H, Ahmed A, Pang Y, Klinkova A: **Interplay of Electrochemical and Electrical Effects Induces Structural transformations in Electrocatalysts.** *Nat. Catal.* 2021, **4**:479–487 https://doi.org/10.1038/s41929-021-00624-y.

59. Frenkel-Mullerad H, Avnir D: **Sol-Gel Materials as Efficient Enzyme Protectors: Preserving the Activity of Phosphatases under Extreme pH Conditions.** *J. Am. Chem. Soc.* 2005, **127**: 8077–8081 https://doi.org/10.1021/ja0507719.

60. Schlager S, Dumitru LM, Haberbauer M, Fuchsbauer A, Neugebauer H, Hiemetsberger D, Wagner A, Portenkirchner E, Sariciftci NS: **Electrochemical Reduction of Carbon Dioxide to Methanol by Direct Injection of Electrons into Immobilized Enzymes on a Modified Electrode.** *ChemSusChem.* 2016, **9**:631–635 https://doi.org/10.1002/cssc.201501496.

61. Gustavsson M, Zheng Y, Handel TM: **Chapter Eleven - Production of Chemokine/Chemokine Receptor Complexes for Structural Biophysical Studies.** *Methods Enzymol.* 2016, **570**:233-260 https://doi.org/10.1016/bs.mie.2015.10.003.

62. Karim AS, Jewett MC: **Chapter Two - Cell-Free Synthetic Biology for Pathway Prototyping.** *Methods Enzymol.* 2018, **608**:31-57 https://doi.org/10.1016/bs.mie.2018.04.029.

63. Jo BH, Park TY, Park HJ, Yeon YJ, Yoo YJ, Cha HJ: **Engineering De Novo Disulfide Bond in Bacterial α-Type Carbonic Anhydrase for Thermostable Carbon Sequestration.** *Sci. Rep.* 2016, **6**: Article 29322 https://doi.org/10.1038/srep29322.

64. Jin M, Kim S, Sung J, Yeon J, Choi S: **Crystal Structure of a Highly Thermostable α-Carbonic Anhydrase from *Persephonella* Marina EX-H1.** *Mol Cells* 2019, **42**:460–469 https://doi.org/10.14348/molcells.2019.0029.

65. Onbas R, Yesil-Celiktas O. **Synthesis of Alginate-Silica Hybrid Hydrogel for Biocatalytic Conversion by β-Glucosidase in Microreactor.** *Eng Life Sci.* 2019, **19**:37–46 https://doi.org/10.1002%2Felsc.201800124.

66. Xu X, Kentish SE, Martin GJO. **Direct Air Capture of CO_2 by Microalgae with Buoyant Beads Encapsulating Carbonic Anhydrase.** *ACS Sustainable Chem. Eng.* 2021, **9**:9698-9706 https://doi.org/10.1021/acssuschemeng.1c01618.

67. Su DD, Aissou K, Zhang Y, Gervais V, Ulrich S, Barboiu M. **Squalene–polyethyleneimine–dynamic constitutional frameworks enhancing the enzymatic activity of carbonic anhydrase.** *Catal. Sci. Technol.* 2022, **12**:3094-3101 https://doi.org/10.1039/D1CY02290C.

68. Mesbahuddin MS, Ganesan A, Kalyaanamoorthy S: **Engineering stable carbonic anhydrases for CO_2 capture: a critical review.** *Protein Eng. Des. Sel.* 2021, **34**:1-12 https://doi.org/10.1093/protein/gzab021.

Appendix

Supplementary Experimental Results

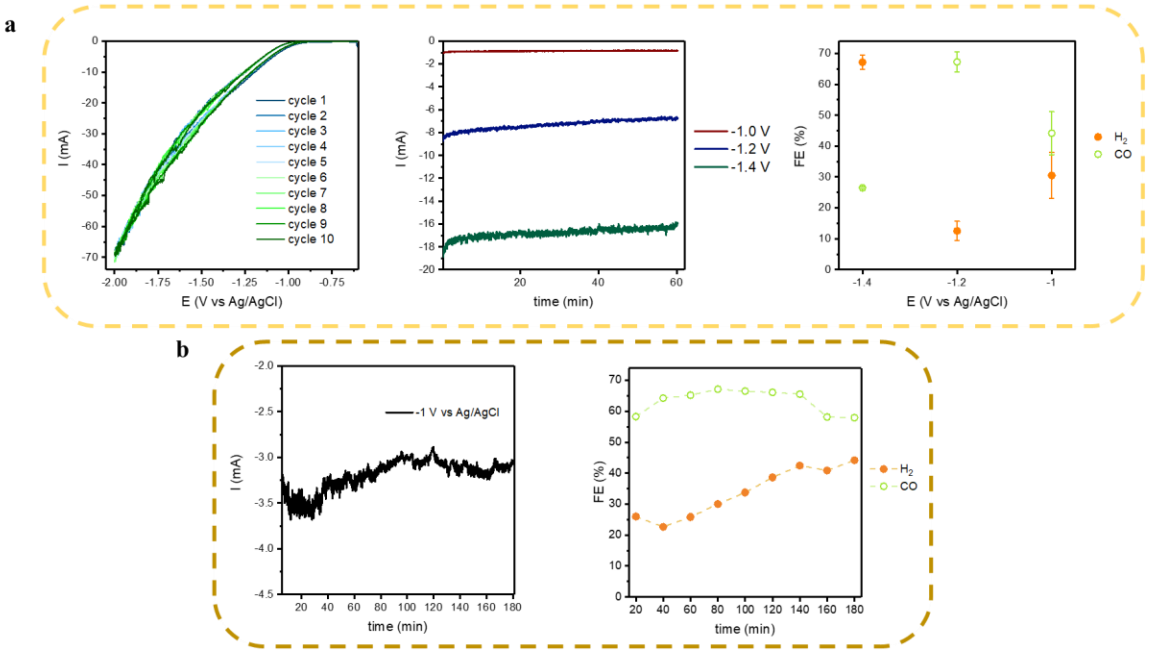

Figure A.1 (a) Electrochemical data including cyclic voltammetry performed with the Au BNPs carbon paper electrode in the CO_2 saturated 0.5 M $KHCO_3$ electrolyte, chronoamperometry performed at -1, -1.2, and -1.4 V vs Ag/AgCl, and the resulting FE for CO and H_2 at each tested potential. (b) Electrochemical data including chronoamperometry performed with the Au BNPs carbon felt electrode in the CO_2 saturated 0.5 M $KHCO_3$ electrolyte and the corresponding change in the FE for CO and H_2 over time.

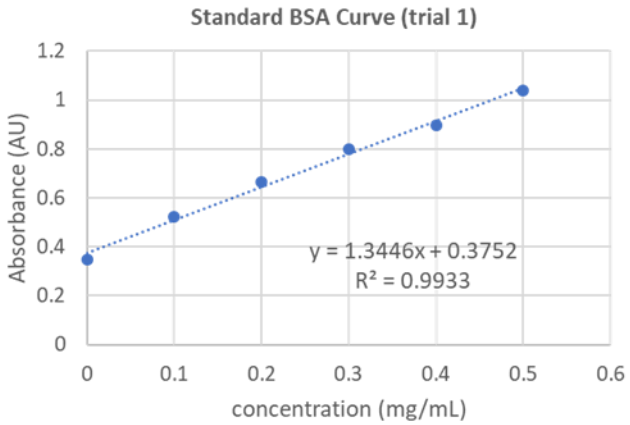

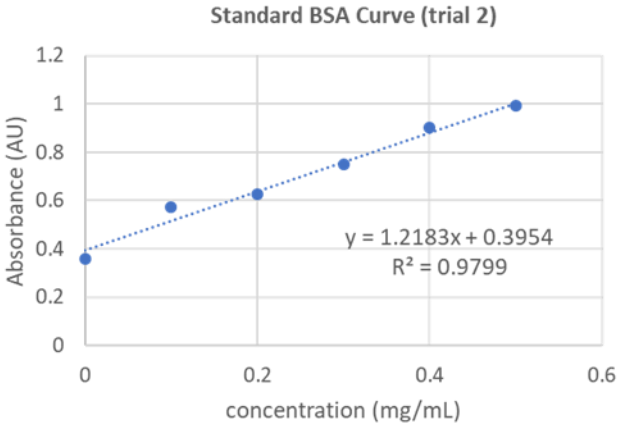

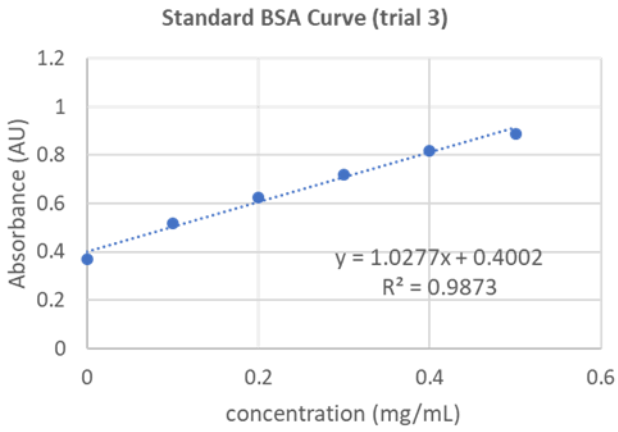

Figure A.2 Standard BSA curves for trials #1-3 of the Bradford assay.